REMIGIJUS JANULIONIS

NUMERICAL RESEARCH OF FRACTURE OF NUCLEAR ENERGY OBJECTS CONSTRUCTION ELEMENTS WITH HYDRIDES UNDER THERMAL IMPACT

SUMMARY OF DOCTORAL DISSERTATION

TECHNOLOGICAL SCIENCES, ENERGETICS AND POWER ENGINEERING (T 006)

Kaunas
2020

KAUNAS UNIVERSITY OF TECHNOLOGY

LITHUANIAN ENERGY INSTITUTE

REMIGIJUS JANULIONIS

NUMERICAL RESEARCH OF FRACTURE OF NUCLEAR ENERGY OBJECTS CONSTRUCTION ELEMENTS WITH HYDRIDES UNDER THERMAL IMPACT

Summary of Doctoral Dissertation
Technological Sciences, Energetics and Power Engineering (T 006)

2020, Kaunas

This doctoral dissertation was prepared at the Lithuanian Energy Institute, Laboratory of Nuclear Installation Safety, during the period of 2015–2019. The studies were supported by Research Council of Lithuania.

Scientific Supervisor:
Dr. Gintautas DUNDULIS (Lithuanian Energy Institute, Technological Sciences, Energetics and Power Engineering, T 006).

Editor: Agnė Lukševičiūtė

Dissertation Defence Board of Energetics and Power Engineering Science Field:
Dr. Raimondas PABARČIUS (Kaunas University of Technology, Technological Sciences, Energetics and Power Engineering, T 006) – **chairman**;
Prof. Dr. Leon CIZELJ (Jozef Stefan Institute, Slovenia, Technological Sciences, Mechanical Engineering, T 009);
Prof. Dr. Habil. Rimantas KAČIANAUSKAS (Vilniaus Gediminas Technical University, Technological Sciences, Mechanical Engineering, T 009);
Prof. Dr. Habil. Gintautas MILIAUSKAS (Kaunas University of Technology, Technological Sciences, Energetics and Power Engineering, T 006);
Dr. Egidijus URBONAVIČIUS (Lithuanian Energy Institute, Technological Sciences, Energetics and Power Engineering, T 006).

The official defence of the dissertation will be held at 2 p.m. on 17 of June, 2020 at the public meeting of Dissertation Defence Board of Energetics and Power Engineering Science Field in the Meeting Hall at the Lithuanian Energy Institute.

Address: Breslaujos str. 3-330, 44403 Kaunas, Lithuania.
Tel. (+370) 37 300 042, Fax (+370) 37 324 144; E-mail: doktorantura@ktu.lt.

Summary of doctoral dissertation was sent on 15 May 2020.
The doctoral dissertation is available on the Internet http://ktu.edu and at the libraries of Kaunas University of Technology (K. Donelaičio str. 20, 44239 Kaunas, Lithuania) and the Lithuanian Energy Institute (Breslaujos str. 3, 44403 Kaunas, Lithuania).

KAUNO TECHNOLOGIJOS UNIVERSITETAS
LIETUVOS ENERGETIKOS INSTITUTAS

REMIGIJUS JANULIONIS

HIDRIDŲ IR TERMINIO POVEIKIO ĮTAKOS BRANDUOLINĖS ENERGETIKOS OBJEKTŲ KONSTRUKCINIŲ ELEMENTŲ IRIMUI SKAITINIS TYRIMAS

Daktaro disertacijos santrauka
Technologijos mokslai, Energetika ir Termoinžinerija (T 006)

2020, Kaunas

Daktaro disertacija rengta 2015 – 2019 metais Lietuvos energetikos institute, Branduolinių įrenginių saugos laboratorijoje. Mokslinius tyrimus rėmė Lietuvos mokslo taryba.

Mokslinis vadovas:
Dr. Gintautas DUNDULIS (Lietuvos energetikos institutas, technologijos mokslai, energetika ir termoinžinerija, T 006)

Energetikos ir termoinžinerijos mokslo krypties disertacijos gynimo taryba:
Dr. Raimondas PABARČIUS (Kauno technologijos universitetas, technologijos mokslai, energetika ir termoinžinerija, T 006) – **pirmininkas**;
Prof. dr. Leon CIZELJ (Jozefo Stefano institutas, Slovėnija, technologijos mokslai, mechanikos inžinerija, T 009);
Prof. habil. dr. Rimantas KAČIANAUSKAS (Vilniaus Gedimino technikos universitetas, technologijos mokslai, mechanikos inžinerija, T 009);
Prof. habil. dr. Gintautas MILIAUSKAS (Kauno technologijos universitetas, technologijos mokslai, energetika ir termoinžinerija, T 006);
Dr. Egidijus URBONAVIČIUS (Lietuvos energetikos institutas, technologijos mokslai, energetika ir termoinžinerija, T 006).

Disertacija bus ginama viešame Energetikos ir termoinžinerijos mokslo krypties disertacijos gynimo tarybos posėdyje 2020 m. birželio 17 d. 14 val. Lietuvos energetikos instituto posėdžių salėje.

Adresas: Breslaujos g. 3-330, 44403 Kaunas, Lietuva.
Tel. (+370) 37 300 042; faks. (+370) 37 324 144; el. paštas: doktorantura@ktu.lt.

Disertacijos santrauka išsiųsta 2020 m. gegužės 15 d.
Su disertacija galima susipažinti internetinėje svetainėje http://ktu.edu, Kauno technologijos universiteto bibliotekoje (K. Donelaičio g. 20, 44239 Kaunas) ir Lietuvos energetikos institute (Breslaujos g. 3, 44403 Kaunas).

CONTENT

INTRODUCTION

According to the World Nuclear Association, there were around 450 nuclear reactors in operation in 2019 which produce around 11 % of all electricity in the world. Also, there are around 60 nuclear reactors under construction which are expected to produce 15 % of electrical energy of currently produced electricity in the world by nuclear power plants (NPPs). However, the age of most reactors that are operated at the moment is in the interval from 30 to 45 years. The design lifetime of Generation II NPPs is 30–40 years, which means that most of NPPs are at the end of their design lifetime. Therefore, to avoid a significant loss of electric power generators by the shutdown of nuclear reactors approaching the design lifetime, EU and other governments aim to extend the service lifetime to 50–60 years by implementing various international projects such as NULIFE (2006–2011), etc. The lifetime extension leads to additional problems with the assurance of safety and reliability of NPPs.

The safety and reliability of nuclear energy objects construction elements remain relevant not only during the operation of the reactor but also during spent nuclear fuel storage when absorbed hydrogen concentrations are sufficient and a mechanism for delayed hydride cracking may occur.

The hydrogen influence on the properties of zirconium alloys is usually evaluated experimentally, however, experimental studies are long-lasting, expensive, and require a sample of the test material. Therefore, alternative research methods are needed. This paper presents a numerical evaluation method of fracture toughness for zirconium alloys where zirconium hydrides are formed due to hydrogen absorption. The developed methodology, using finite element models, allows the evaluation of hydrogen influence on zirconium alloy properties.

Two-dimensional and three-dimensional finite element models were researched for the development of the numerical evaluation method. A numerical study of standard compact tension test specimens has shown that two-dimensional finite element models, in both states, plane strain and plane stress, are not suitable for estimating fracture toughness. Studies have shown that a three-dimensional finite element compact tension specimen model is more suitable for this purpose.

The research of fracture toughness parameters has also revealed that even with a relatively high hydrogen concentration of 140 ppm, the Zr-2.5Nb TMT-2 alloy remains relatively ductile, and only the conditional stress intensity factor K_Q can be determined. Therefore, to evaluate the fracture toughness of this alloy the critical J-integral value J_{IC} has to be found.

In the course of the above-mentioned research, the numerical research method was developed in the thesis. This method can be used to evaluate the mechanical properties and fracture toughness of zirconium alloy depending on hydrogen concentration.

The dissertation was prepared at the Lithuanian Energy Institute, Laboratory of Nuclear Installation Safety, in the period of 2015–2019. The research was done by performing works funded by the Lithuanian state budget: the scientific working group's project "Model of Durability Evaluation of Next-generation Steel" (2014–2016) and the long-term institutional R&D programme "Research on Safety-critical Processes in Nuclear and Thermonuclear Installations" (2012–2016), as well as working on the Incefa + project (2015–2020) funded by the European Union Horizon 2020 programme.

Relevance of the research

Nuclear fuel claddings are made of zirconium alloy, which, in addition to the ageing mechanisms of other metals, is also susceptive to hydrogen absorption and it following delayed hydride cracking mechanisms. After the exploitation, nuclear fuel with its cladding is stored in spent fuel pools, short-term storage containers, and then disposed of in deep geological repositories. In all cases, the reliability of the fuel cladding is important, the structural integrity and leak-proof must be ensured.

Usually, the effects of the ageing of materials are evaluated by laboratory tests. As fuel claddings are a protective measure to prevent the release of radioactive fission products into the environment, their experimental studies are complex, difficult, and costly. Therefore, alternative methods are needed for the material ageing assessment.

As well as fuel claddings the fuel channels of channel type nuclear reactors are made of zirconium alloy. Therefore, they are subject to the same ageing mechanisms. Ageing mechanisms have a significant impact on the reliability of fuel channels and the whole nuclear reactor.

Aim of the research

To determine the fracture toughness of nuclear energy objects construction elements made of zirconium alloy with hydrides under thermal impact using the developed numerical method.

Tasks of the research

1. Experimentally measure the dimensions of zirconium hydrides at different hydrogen concentrations;
2. Develop a numerical modelling method and determine the mechanical properties of the material with hydrides;
3. Develop a numerical modelling method and determine the critical stress intensity factor value of zirconium alloy with hydrides;
4. Develop a numerical modelling method to determine the growth of the crack in a compact tension specimen;

5. Develop a numerical modelling method and determine the critical value of the J-integral of a zirconium alloy with hydrides.

Novelty of the work

A new numerical simulation methodology has been proposed, which allows numerical determination of fracture toughness of zirconium alloys at different hydrogen concentrations.

The crack growth determination methods were supplemented with the proposed and validated polynomial equation.

Practical significance of the research

The developed methodology is suitable for the determination of critical stress intensity factor and J-integral values of various metal alloys. By applying this methodology for the structural elements of nuclear energy object made of zirconium alloys, i.e. fuel channels and fuel claddings, it is possible to predict a change in their properties due to the hydrogen absorption mechanism during the operation of a reactor or the storage of spent nuclear fuel, which increases the reliability of the entire nuclear power plant. It is also very relevant during the storage of spent nuclear fuel, as the amounts of hydrogen concentration in the fuel cladding accumulated during the operation are high and the temperatures are sufficient for the mechanism of delayed hydride cracking to occur. Therefore, using this methodology, it is possible to improve the design of fuel claddings and spent fuel storage procedures.

Evaluating the influence of irradiation on the properties of zirconium alloy, the developed methodology is also suitable for the assessment of fracture toughness of irradiated materials of structural elements under hydrides and thermal impact.

Statements presented for defence

1. Along with the increase of hydrogen concentration in the zirconium alloy the thickness, length, and volume part of zirconium hydrides is also increasing.
2. Using a two-dimensional finite element model of one medium-sized hydride surrounded by zirconium matrix the mechanical properties of hydride material can be determined.
3. Three-dimensional finite element model using standard compact tension specimens is more suitable for the determination of critical fracture toughness value than the two-dimensional model.
4. Using the determined second-order polynomial equation the crack growth in compact tension specimen can be evaluated.
5. Using the developed numerical model the critical values of J-integral of zirconium alloy with hydrides can be determined.

Author's contribution to the analysed problem

Remigijus Janulionis is a Junior Research Associate in the Lithuanian Energy Institute, Laboratory of Nuclear Installation Safety. He developed the method for the numerical determination of fracture toughness of zirconium alloys with hydrides. For this purpose, he experimentally measured the dimensions and volume part of zirconium hydride in zirconium matrix and developed a numerical method for the determination of mechanical properties of zirconium alloy with hydrides. For the development of a numerical method for fracture toughness determination, he was involved in the planning of experimental research of critical stress intensity factor and critical J-integral of steel P91 and the discussion of the obtained experimental results. Using the data obtained in these experimental tests he developed a numerical method for evaluation of fracture toughness of steels as well as zirconium alloys.

Approbation of dissertation

1 scientific article on the theme of the dissertation has been published in the journal with citation index at *Clarivate Analytics* database *Web of Science Core Collection* and 1 article in the journal referred to in the international scientific database. Results of the research were presented in 1 conference held in a foreign country and 5 international conferences in Lithuania. 5 articles were published in conference proceedings.

Structure and content

The dissertation consists of an introduction, literature review, measurement method description, descriptions of numerical research method and model, numerical research results and discussion, application of the numerical methodology in the case of zirconium alloy hydrides, conclusions, references, and list of scientific publications. The thesis consists of 104 pages, including 79 pictures, 9 tables, 103 references.

1. LITERATURE REVIEW

The literature review has shown that various zirconium alloys during ageing do absorb hydrogen. When the concentration of absorbed hydrogen in zirconium alloys exceeds the solubility limit the zirconium hydrides start to form. Hydrogen absorption does often lead to delayed hydride cracking (DHC) mechanism. Both of these mechanisms affect the mechanical properties of the zirconium and its alloys and their plasticity, which directly affects the material's resistance to fracture, i.e. the material fracture toughness properties.

The literature review also showed that hydrogen absorption and DHC mechanisms remain relevant during the spent nuclear fuel (SNF) storage when the heat release of the spent fuel tablet decreases and the temperature of the fuel claddings drops to a level where the DHC mechanism is intense. Therefore, in the long term, the hydrogen absorption ageing mechanism in fuel claddings should be considered during the nuclear fuel operation in reactor and storage of SNF. During the long time period, the change of mechanical and fracture toughness properties of zirconium alloys has to be determined to ensure the safety of the SNF.

Zirconium alloys differ not only in their chemical composition but also in thermo-mechanical treatment during the manufacturing process. All of this does affect the mechanical properties of zirconium alloys and the geometry of zirconium hydrides which are by formed due to hydrogen absorption and thermal impact. The literature review has shown that the hydride size also depends on the cooling rate of zirconium alloy. Therefore, in order to carry out the research on zirconium alloy with hydrides, in the first place, it is necessary to determine the dimensions of the hydrides, i.e. width, length, and the volume part in zirconium matrix.

Most of the research on the properties of zirconium alloys are carried out by experimental test. However, experimental tests of materials are not always possible. In particular, a sample of the material is required for the preparation of test specimens. The material must be taken from an existing nuclear reactor or SNF storage facility, which itself is a complex operation. The volume of gathered material must be relatively substantial since experimental samples must be of standard dimensions. Often, nuclear materials are irradiated, and to test such materials special hot laboratories are required. All of this makes experimental research difficult and expensive. Therefore, alternative methods of material research are necessary to determine the changing properties of materials and to ensure the safety of nuclear installations. As an alternative to experimental research, the numerical studies of materials have been found in the scientific literature, for which the finite element method is commonly used. Although articles on the numerical determination of critical fracture parameters of zirconium alloys could not be found, the descriptions of numerical research of critical fracture parameters of other metals are available. However, the use of these methods

requires additional experimental tests, therefore, a new suitable numerical method has to be developed in order to evaluate the fracture toughness of nuclear energy objects construction elements with hydrides.

It is impossible to investigate all zirconium alloys within the scope of the dissertation, therefore, application of the proposed numerical methodology was performed for the Zr-2.5Nb RBMK TMT-2 alloy.

2. METHODOLOGY OF NUMERICAL EVALUATION OF FRACTURE TOUGHNESS

The main aim of the dissertation is to determine the fracture toughness of nuclear energy objects construction elements made of zirconium alloy with hydrides under thermal impact using the developed numerical method. To achieve the aim, the tasks of the research formed at the beginning of the dissertation must be solved by carrying out the work stages according to the algorithm presented in Fig. 2.1.
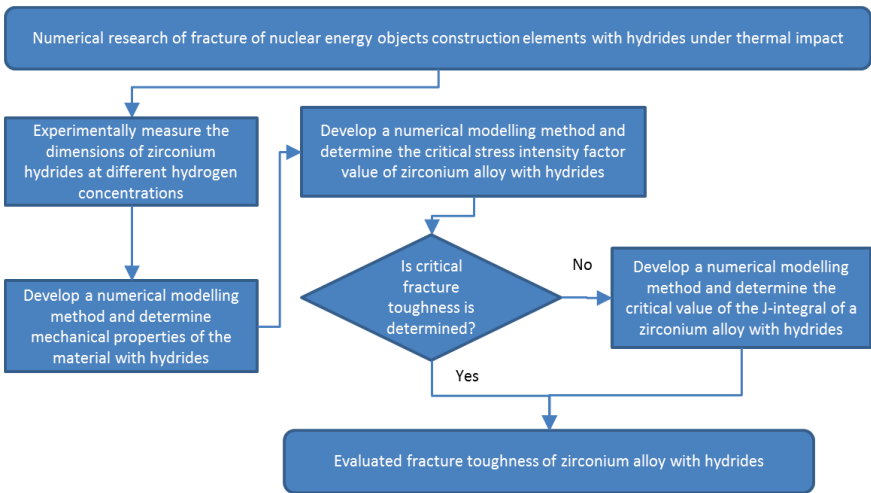
Fig. 2.1. Algorythm of research methodology

Searching the scientific literature in the field of fracture toughness numerical modelling, some articles, where the J_{IC} values were determined by applying the finite element method were found. The papers show a good agreement with experimental data, therefore, numerical research using finite element method (FEM) was also chosen for the evaluation of fracture toughness of zirconium alloys with hydrides. To describe the behaviour of created finite element (FE) models under load the material properties have to be described.

Therefore, firstly, the mechanical properties of the zirconium alloy with hydrides must be numerically evaluated. Undoubtedly, different dimensions of the zirconium hydride in the zirconium alloy will have different effects on the mechanical properties of the zirconium alloy. As shown in the literature review, the shape of the hydrides depends not only on the composition of the zirconium alloy but also on the mechanical and thermal treatment. Therefore, to evaluate the size and shape of hydrides in the Zr-2.5Nb TMT-2 alloy they were measured using direct measurements.

2.1. Research object and preparation of specimens

Ignalina NPP fuel channel (FC) was selected for the research of zirconium alloy, which has been subjected to thermal-mechanical treatment according to the TMT-2 technology. The part of the unirradiated FC tube made of the Zr-2.5Nb alloy was obtained from Ignalina NPP (Fig. 2.2). The FC obtained for the tests was 1.5 m long, with an outside diameter of Ø 88 mm, and a wall thickness of ~4 mm. The FC pipe section was divided into 20 segments.
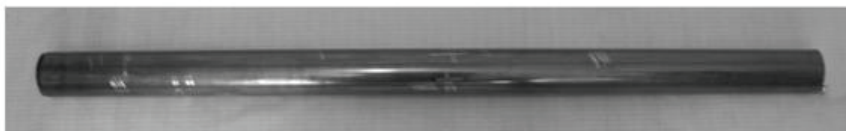
Fig. 2.2. A part of Ignalina NPP fuel channel used for the research

Preparation of specimens with hydrides was performed in the Laboratory of Materials Research and Testing at the Lithuanian Energy Institute. The FC segments were prepared by electrolytically depositing the zirconium hydride layer and homogenizing it at a set temperature. In this way, hydrogen is diffusely distributed in the sample volume from the formed zirconium hydride layer. For hydrogenation, a 0.2 M = 0.2 mol/L sulfuric acid solution at 70 °C at a current density of 1-2 A/m2 was used. According to [1], the minimum hydride layer for the required hydrogen concentration is found by the equation:

$$t_{hidrido} = 7.322 \cdot 10^{-5} \cdot t_{Zr} \cdot [H]_{Zr} \tag{1}$$

here $t_{hidrido}$ – the thickness of hydride layer, m; $[H]_{Zr}$ – hydrogen concentration, ppm; t_{Zr} – thickness of zirconium specimen, m.

To ensure a sufficient amount of hydrogen, a 50% thicker hydride layer was applied to the surface of the FC segments than determined by equation (1). The obtained thickness of the zirconium hydride layer and the uniformity of the hydride distribution in the zirconium alloy volume after the homogenisation is verified metallographically.

The sample with the formed hydride layer is homogenised by maintaining the temperature for a fixed time at elevated temperature and due to the hysteresis

of hydrogen solubility at changing temperature, the elemental hydrogen is diffusely distributed throughout the sample as the hydride layer melts. Subsequently, the temperature is lowered and new hydrides are formed. The temperature of the homogenisation is calculated using equation [1]:

$$[H]_{Zr} = 1.2 \cdot 10^5 exp(-Q/RT), \tag{2}$$

here Q – process activation energy, J/mol; R – universal gas constant, J/(mol·K).

When the hydride layer is on both sides of the specimen the homogenisation time can be found using equation [1]:

$$h_h = 1.5(t_{Zr}/2)^2/D, \tag{3}$$

where D – diffusion coefficient, m²/s and is found according to equation [2]:

$$D = 7.0 \cdot 10^{-7} exp(Q/RT)^2. \tag{4}$$

The size of the hydrides formed in the zirconium alloy depends on the cooling rate of the alloy. Therefore, it is important to select the conditions correctly that you want to imitate when forming the hydrides. After the completion of the homogenisation process, the cooling rate of the samples of 30 °C/h was selected. That coincides with the cooling rate of the FC during the emergency shutdown of the RBMK reactor.

The morphology of the formed hydrides and the microstructure of the alloy were investigated metallographically using an optical microscope with an automatic image analysis system, and a SEM microscope. Hydrogen analysis was performed by vacuum extraction on a LECO RH-402 instrument.

2.2. Measurement of hydride size in zirconium alloy

During the examination of microsection photos of the Zr-2.5Nb alloy with hydrides (Fig. 2.3) it was noticed that different hydride concentration in the zirconium alloy not only results in higher number but also different lengths and widths of hydrides.

To develop a methodology for the determination of the change of the properties of zirconium alloys with hydrides, it is necessary to determine the dimensions of the hydrides. It can be seen in Fig. 2.4 that the hydrides of the Zr-2.5Nb alloy FC with TMT-2 thermo-mechanical treatment do penetrate perpendicular to the inner and outer surfaces of the pipe, but tend to form in axial-tangential (axial-circumferential) direction in the centre layers of the pipe. This hydride formation tendency is also observed in the pressurised heavy water reactor type pressure pipes [3]. This orientation of the zirconium hydrides depends on the FC crystallographic texture that formed during the processing technology of TMT-2.

14
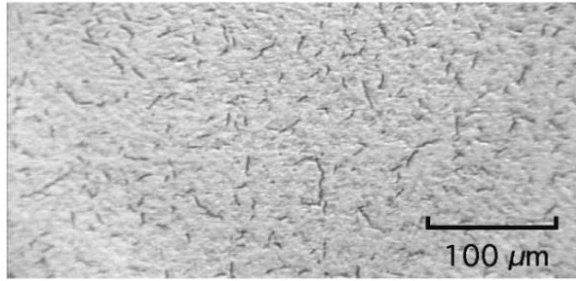
a)
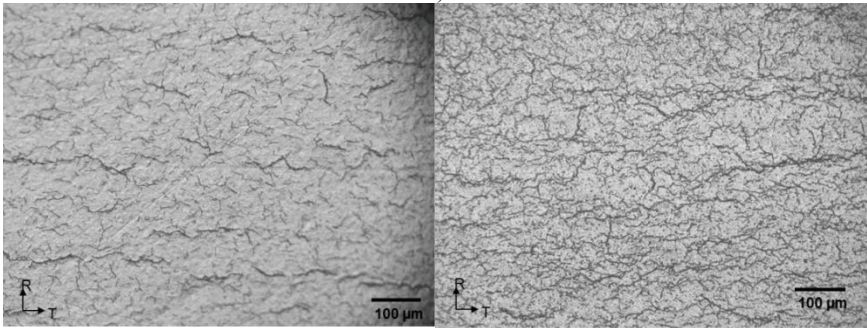
b)   c)

Fig. 2.3. Microstructure of Zr-2.5Nb alloy FC in radial-tangential direction at different hydrogen concentrations: a) 45 ppm; b) 100 ppm; c) 250 ppm
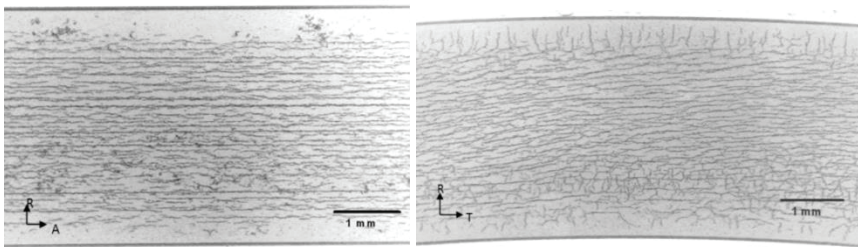
a)   b)

Fig. 2.4. Hydride distribution and orientation in the Zr-2.5Nb alloy FC at a hydrogen concentration of 140 ppm: a) cross-section in radial-axial direction; b) cross-section in the radial-tangential direction

The lengths of hydride in zirconium alloy were determined by direct measurements from microsection photos of the Zr-2.5Nb alloy FC (Fig. 2.3). The lengths of zirconium hydrides were measured in samples with hydrogen

concentrations of 45, 100, and 250 ppm. The computer-aided design programme AutoCAD LT 2011 [4] was used for the measurements.

Hydride size measurement results are presented in Section 3.1.

To measure the length and width of the average hydride is not sufficient to determine what part of the zirconium matrix does a hydride occupy. Therefore, the additional measurement of the hydride volume part in the zirconium alloy matrix is described in Section 2.3.

2.3. Determination of hydride volume part

The hydride volume part in obtained zirconium alloy specimens was determined from the prepared microsection photos using a stereologic planimetric method [5]. Using this method it is assumed that in any cross-section of the specimen the area occupied by chaotically located hydrides is the same. If this condition is adopted, the relative area occupied by the hydrides can be equated to the relative volume part.

The hydride occupied volume part in the zirconium alloy matrix and their dimensions are later used for numerical simulation of properties of zirconium alloy with hydrides.

The photos of the test specimens' surfaces were taken by an optical microscope OLYMPUS at magnifications of 150 and 800 times. Images processed and hydride volume calculations were performed with a computer programme Scion Image v.4.0.2. An example of a microsection photo analysis with the programme Scion Image is shown in Figure 2.5. Surface analysis was performed at random locations of the specimen in two cross-section planes: axial-radial (A-T) and radial-tangential (R-T). At least 10 measurements were taken in each plane and for each hydrogen concentration.

The results of the determination of the hydride volume part in the zirconium matrix are presented in Section 3.1.

a)   b)

c)
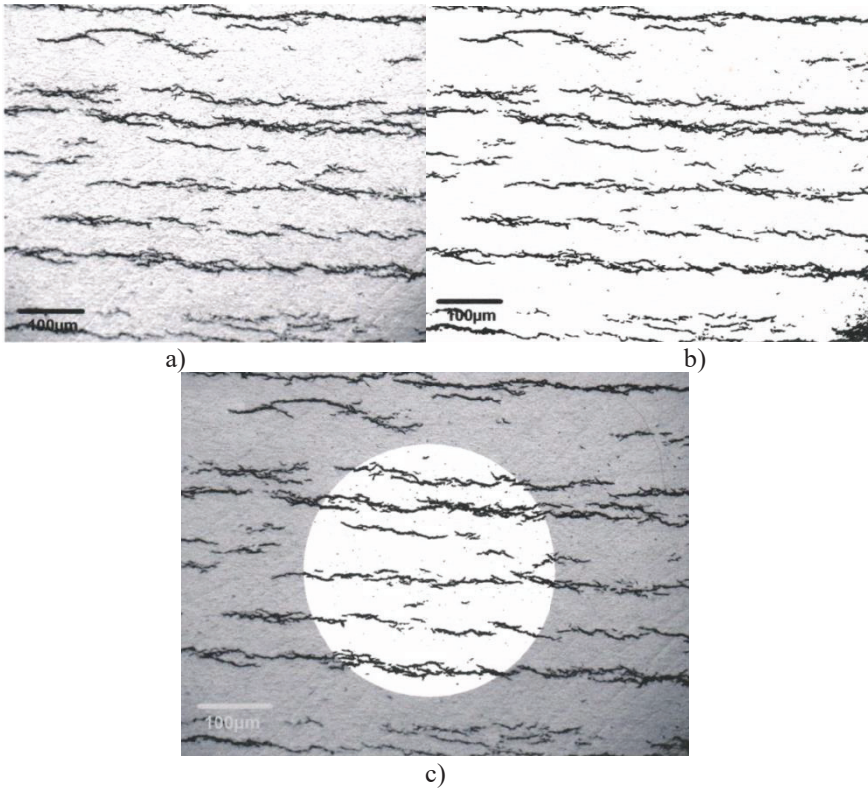
Fig. 2.5. Microsection photo automated processing using image analysis programme
Scion Image at a hydrogen concentration of 137 ppm: a) image of microsection surface;
(b) binary image; (c) measuring surface area (0.17 mm^2)

2.4. Numerical evaluation of mechanical properties of zirconium alloy with hydrides

2.4.1. Numerical model of zirconium alloy with hydride for the evaluation of mechanical properties

As shown in Section 2.2, hydrides in FC of Zr-2.5Nb with TMT-2 treatment tend to form in the axial-tangential direction (Fig. 2.4.). Also, during the FC operation, the highest stresses occur in the circumferential direction of the tube, therefore, both experimental research [3], the dissertation results are compared with, and numerical research are performed in the circumferential (tangential) direction of the tube.

The principle of the numerical determination of the mechanical properties of zirconium alloy with hydrides is a numerical simulation of an experiment in

micro scale. It is assumed that the behaviour of one average size hydride surrounded by a zirconium alloy matrix under uniaxial loading corresponds with a behaviour of 37.8 mm long tensile test specimen made of FC tube. In the experimental specimen, the hydrides are oriented directionally but not uniformly spaced, and their dimensions are different. This has different effects on the properties of the material at individual locations in the sample at the micro scale, whereas at the macro scale the evaluation is made for the whole system, i.e. the experiment gives the average of the different properties of the material in separate volumes. Therefore, the analysis of an average size hydride surrounded by a zirconium matrix yields average material properties as in the experimental study. The micro model shows how one average size hydride, without interaction with other hydrides, does change the properties of the zirconium alloy and hydride system. Therefore, the orientation of the hydride and the loading in the numerical model must coincide with the loading direction and the orientation of the specimen of the experimental studies.

A numerical model of a zirconium alloy matrix with a hydride insert created by ABAQUS is shown in Fig. 2.6 a. The figure shows the zirconium matrix and hydride models at hydrogen concentrations of 52, 100, and 140 ppm. The dimensions of the modelled hydride correspond to those of the average hydride measured experimentally (Fig. 3.1). For the corresponding hydrogen concentration, the modelled hydride has a length ranging from 18.8 to 27.7 μm and width from 2.3 to 6.7 μm. The zircon matrix is modelled in the shape of a regular square. The edge length of the zirconium matrix was chosen so that the area occupied by the hydride, which coincides with the hydride volume fraction in the zirconium alloy, corresponds to the hydride volume measurement results (Fig. 3.2 and Table 3.1). The thickness of the created model is equal to 1 μm. The end of the modelled hydride is rounded to avoid stress concentration. As the model of one hydride surrounded by a zirconium matrix is symmetric with respect to two planes, only 1/4 of the hydride and zirconium alloy is modelled with the purpose to reduce the size of the numerical model, the number of finite elements, and to speed up the calculations. Symmetry boundary conditions were added at the intersections of the symmetry planes in the model with the lower horizontal and right vertical edges (Fig. 2.6 a). The displacement was used as a load and was added to the top horizontal edge. The size of the added displacements is 3 μm for all models. This magnitude of displacement is sufficient to calculate stresses and strains beyond the experimentally determined strength limits of zirconium alloys with hydrides. As a result of the calculation, the reaction force was measured and recalculated to the stresses required to form the stress-strain curve.
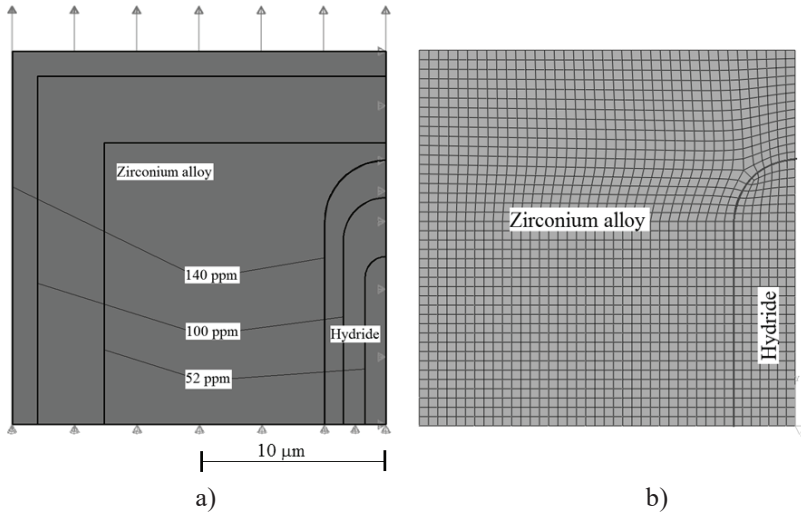
Fig. 2.6. Numerical model and FE mesh of zirconium alloy with hydride: a) geometry and boundary conditions at hydrogen concentrations of 52, 100, and 140 ppm; b) finite element mesh at a hydrogen concentration of 140 ppm

The numerical model is meshed using S8R type elements. These elements are shell type with 8 nodes [6]. Each element node has 6 degrees of freedom and 5 integration points across the thickness of the element. To select the optimal FE size, several calculations were performed using different element sizes (0.1 μm, 0.2 μm, 0.5 μm, 1 μm, 2 μm). As the model has a simple geometry, the load is uniaxial, the size of the elements, when the model is divided into relatively small elements, has no significant impact on the calculation results. Therefore, for all cases, the numerical model was meshed using 0.5 μm size elements. The FE model mesh at 140 ppm hydrogen is shown in Fig. 2.6 b.

2.4.2. Mechanical properties of zirconium alloy and hydride

The mechanical properties of the zirconium alloy used in the numerical model are presented in Table 2.1. The table shows the modulus of elasticity E, the relative yield strength $\sigma_{0.2}$, the ultimate strength σ_U, the failure strain ε_f, and the reduction of the sample cross-sectional area Z. These mechanical properties were found in the literature [3], where the FC of Ignalina NPP made of the Zr-2.5Nb alloy was investigated.

Table 2.1. Mechanical properties of the Zr-2,5Nb alloy [3]

E, GPa	$\sigma_{0.2}$, MPa	σ_U, MPa	ε_f, %	Z, %
34.4	411	492	14.78	62.2

Mechanical properties of zirconium hydride were calculated according to the method presented in [4]: modulus of elasticity E (Pa) is found by equation:

$$E = (95900 - 57.4 \cdot (T - 273)) \cdot 10^6, \tag{5}$$

here T – temperature, K.

The ultimate strength of zirconium hydride is found by equation:

$$\sigma_U = 7.357 \cdot 10^{-3} E. \tag{6}$$

The founded modulus of elasticity and ultimate strength can be used for the reconstruction of the stress-strain curve of a hydride. The true stress-strain curves of zirconium hydride and the Zr-2.5Nb alloy are presented in Fig. 2.7.
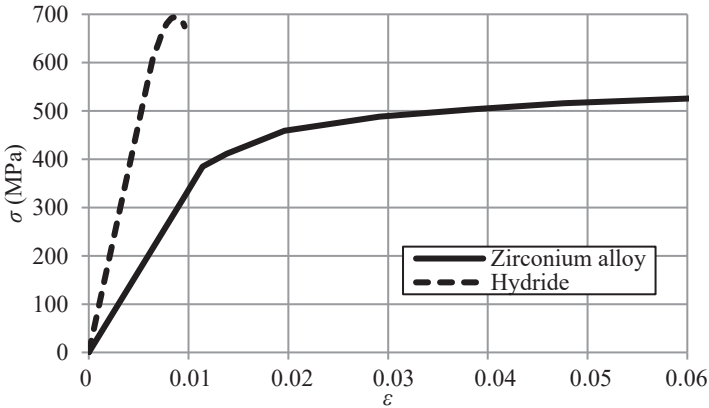

Fig. 2.7. True stress-strain curves of the zirconium hydride and the Zr-2.5Nb alloy

2.5. Evaluation method of fracture parameters

To evaluate the mechanical resistance of materials to fracture under static or cyclic loads is one of the most important tasks of fracture mechanics. Metal components under cyclic load are failing mainly due to flat defects called cracks. There are two types of fractures. The first is the case where there are large residual deformations and the second is the presence of very little or no permanent deformation. Depending on this, the fracture of the material is called plastic or brittle. Based on those two cases of fracture mechanics [5], two theories are distinguished:

- Linear fracture mechanics;
- Nonlinear fracture mechanics.

Linear fracture mechanics is based on the linear elastic behaviour of the material, where plastic strains are only possible in a small part of the material and close to the tip of the crack. Linear fracture mechanics only applies to structures

20

where the nominal stresses do not exceed 40% of the elastic limit. Nonlinear fracture mechanics is not limited by the elastic strain. The plastic strain can take the entire cross-section of the structure. For these two cases of decomposition mechanics, different fracture evaluation parameters are used. To evaluate the crack in linear fracture mechanics the stress intensity factor K_I parameter is used and in nonlinear fracture mechanics – the J-integral parameter. To use these parameters as the criteria their critical values must be found.

2.6. ABAQUS program validation for calculation of fracture parameters

To validate programme ABAQUS FE [6] in solving the fracture mechanics problems the calculation of stress intensity factor of cracks in the Es-Salam reactors vessel was performed. The validation itself was carried out using a method of comparison [7] by comparing the determined stress intensity factors obtained by the programmes ABAQUS and ANSYS [8], and analytical calculations according to ASME [9] requirements.

The Es-Salam reactor is a 15 MW heavy water research reactor. The reactor is located near Birin, 200 km south of the Algerian capital. The reactors pressure vessel is schematically shown in Fig. 2.8.
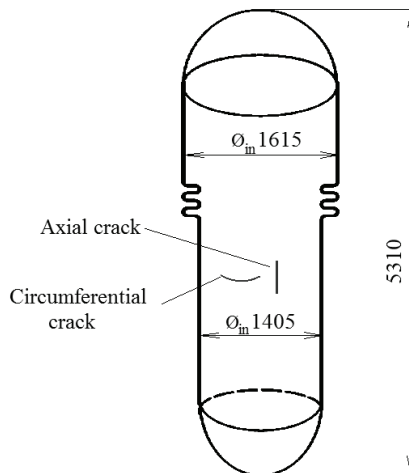

Fig. 2.8. Pressure vessel of the Es-Salam reactor

Internal cracks of different dimensions were evaluated in the analysis, where a depth a and a vessel wall thickness t ratio varies from 0.25 to 0.8, and a crack depth and length c varies from 0.2 to 1.0.
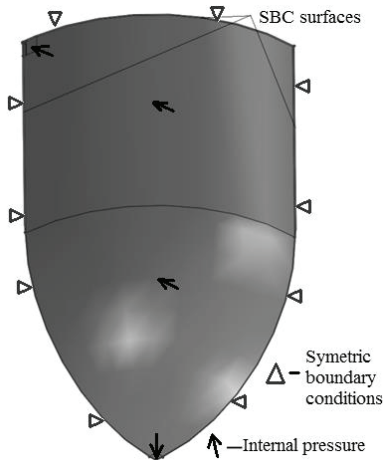
The Es-Salam reactor pressure vessel is made of aluminium 6061 alloy. This aluminium alloy has a modulus of elasticity $E = 75100$ MPa, a Poisson ratio of $\upsilon = 0.33$. The lower part of the pressure vessel has an internal diameter of 1405 mm and a wall thickness of 8 mm. It is assumed that the inner pressure of the vessel is 0.07 MPa.

2.6.1. Analytical stress intensity factor evaluation

Analytical stress intensity factor evaluation was done according to SME Boiler & Pressure Vessel Code Section XI Appendix A-3000 [9]. According to this method the stress intensity factor K_I is calculated by evaluating membrane and bending stresses. Using this method stress intensity factor can be determined in the deepest point of the crack and at the point where the crack front meets the pressure vessel surface, i.e. when the angle at the crack front is respectively equal to $\Phi = 0°$ and $\Phi = 90°$. For the ABAQUS validation, the comparison was made at the deepest point of the crack where $\Phi = 90°$.

2.6.2. Numerical model of the Es-Salam reactor pressure vessel prepared with the ABAQUS

The created FE model of the Es-Salam pressure vessel with applied boundary conditions is shown in Fig. 2.9. The model presents a 1/8 part of the pressure vessel. For the 1/8 part model to correspond to the behaviour of the whole model, the symmetry boundary conditions (SBC) were applied to the 1/8 model cut surfaces. The pressure of 0.07 MPa was applied to the inner surfaces of the model.

Fig. 2.9. FE model of the 1/8 Es-Salam reactor pressure vessel with applied boundary conditions created with the programme ABAQUS

The biggest part of the model is meshed using C3D8R type elements, the size of which was 25 mm (Fig. 2.10). C3D8R is a cubic-shape three-dimensional 8-node element. The crack is modelled in the corner of the model where symmetry conditions are applied (Fig. 2.10 a) and b)). Therefore, only 1/4 of the crack was modelled. Also, in this corner, a 60×60 mm zone was meshed using C3D20R elements. These are three-dimensional brick-shape 20-node elements. The mesh size of this zone was 1 mm.
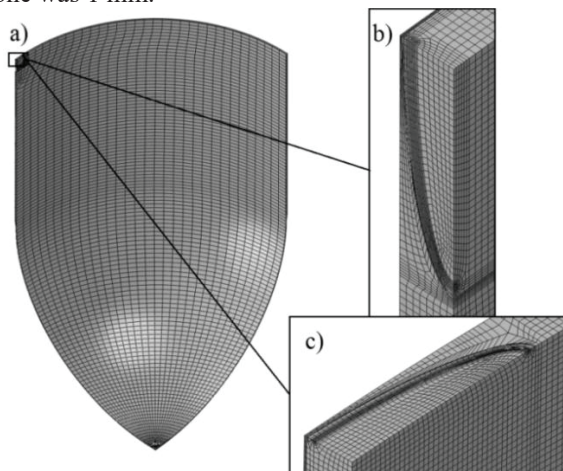
Fig. 2.10. FE mesh of the model with crack ($a = 6{,}4$ mm, $c = 32$ mm): a) whole model mesh; b) increased view of axial crack mesh; c) increased view of the circumferential crack mesh

The FE model creation and calculation using the programme ANSYS was performed by Djillali Saad, a researcher at the Birine Nuclear Research Centre (Algeria). A description of the model and the results obtained are described in a joint publication [10].

Validation of fracture parameters calculation in the programme ABAQUS is presented in Section 3.3.

2.7. Critical K_{IC} evaluation

The principle of numerical investigation of the critical stress intensity factor K_{IC} is the numerical modelling of an experiment according to standard procedures and requirements for the experimental determination of K_{IC}. The requirements of ASTM E399-12e3 [11] have been selected for this purpose. To develop the numerical method for critical K_{IC} determination the experimental test of mechanical and fracture toughness properties of steel P91 was selected. Selected experiments were performed by the Lithuanian Energy Institute's scientists [12].

2.7.1. Experimental research of mechanical properties and stress intensity factor of steel P91

Experimental research of steel P91 was conducted not only for as-received material but also for the aged material. The ageing was carried out by maintaining the specimens at high temperatures for a long period of time, thus simulating the long term high-temperature operation of the components of the electric power industry, as, during the operation, the ageing of the steel does change its microstructure, mechanical and ductile properties. In these tests, the ageing of the steel P91 was performed at different temperatures while maintaining the specimens at different times. The research results of the aged steel P91 at 650 °C for 790, 4150, and 11000 hours were selected for the development of the numerical modelling method for the critical stress intensity factor determination. The design temperature of the Generation IV liquid sodium-cooled reactor is 550 °C, thus, according to the ageing time conversion method presented in [12], the steel P91 aged at 650 °C for 11000 hours, which approximately corresponds to service time of 60 years at 550 °C.

Experimentally determined mechanical properties of as-received and aged steel P91 are presented in Table 2.2. Experimental test results of fracture toughness are presented in Table 2.3. The tests for mechanical properties were carried out in accordance with EN ISO 6892-1 2009 [13] and the tests for fracture toughness according to the ASTM E399-12e3 [11].

Table 2.2. Mechanical properties of as-received and aged steel P91 [12]

Ageing time 650 °C, hours	E, GPa	$\sigma_{0.2}$, MPa	σ_U, MPa	ε_f, %	υ
0	214	513	666	9.8	0.3
790	212	507	658	9.9	0.3
4150	212	501	651	9.5	0.3
11000	209	487	637	9.2	0.3

Table 2.3. Fracture toughness test results of as-received and aged steel P91 [12]

| Ageing time 650 °C, hours	P_Q, kN	P_{max}, kN	K_Q, MPa√m	K_{max}, MPa√m
0	42.4	82.7	75.1	146.4
790	41.4	81.3	73.4	143.5
4150	41.9	78.0	73.9	137.5
11000	41.1	77.0	70.6	135.8

2.7.2. Two-dimensional model for the numerical research of K_{IC}

The principle of numerical research of critical stress intensity factor K_{IC} is the numerical simulation of an experimental test. The two-dimensional model of

the compact tension C(T) specimen was created using the finite element programme ABAQUS and is shown in Fig. 2.11. The dimensions of the numerical model correspond to those of the standard C(T) specimen used for experimental studies [12]. The length of the fatigue crack a_l is 1.8 mm. The two-dimensional finite element models are usually meshed using either CPE8R or CPS8R elements [6]. Both types of elements are flat two-dimensional rectangular with 8 nodes, but one of them evaluate the plane strain and the other – plane stress state. To develop a method for critical stress intensity factor numerical determination both types of elements were used. The area around the crack was meshed using a circular pattern where at the tip of the crack singular elements were used.

The boundary conditions of the FE model were applied to the centres of the holes, marked RP. The displacements of the bottom RP point are constrained in two directions (along the X and Y coordinates), while the displacements of the top RP point are restricted only in the X-coordinate direction. The displacement along the Y-coordinate of the top RP point was used as a load. RP points are connected to the FE model by rigid coupling. The Nlgeom (Nonlinear Geometric Effects) option has been activated in the ABAQUS to evaluate large deformations and displacements [6].

After the calculation, the following results were obtained: reaction force at the bottom RP point, crack opening displacement (COD), which was determined by measuring the displacement of extensometer attachment points Δv and the stress intensity factor at the crack tip.
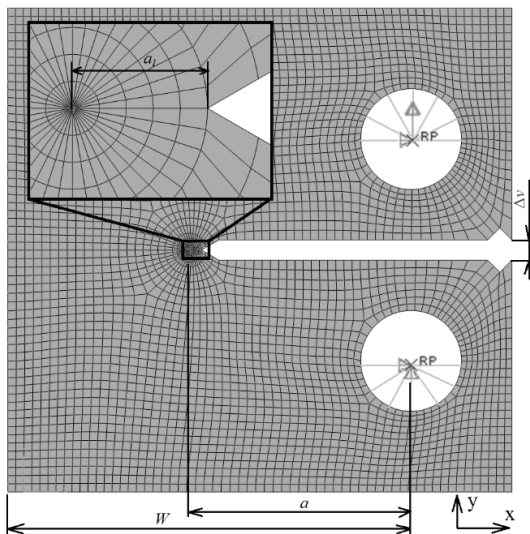
Fig. 2.11. Mesh and boundary conditions of two-dimensional C(T) specimen model

To describe the behaviour of steel P91 the stress-strain curve (Fig. 2.12) was used.
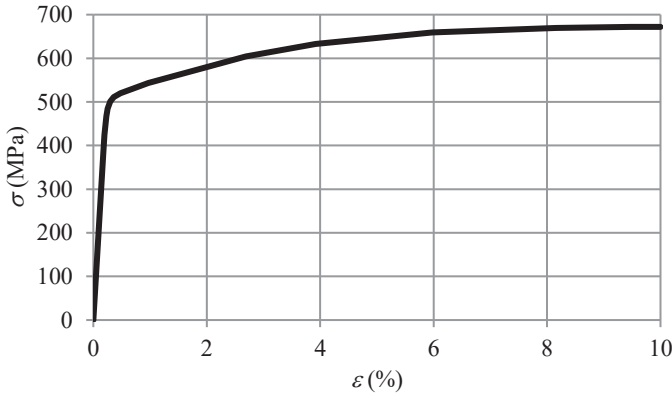

Fig. 2.12. Engineering stress-strain curve of as-received steel P91

The numerical determination of the critical stress intensity factor K_{IC} using the finite element method requires two simulations of the C(T) specimen tension:

- The first C(T) specimen tension simulation is used for the tension force F vs. crack opening displacement v curve creation and determination of P_Q load. For this case nonlinear analysis is performed;
- The second tension simulation is used for the stress intensity factor vs. tension force curve creation and the determination of conditional stress intensity factor K_Q. In this case, the linear analysis is performed.

2.7.3. Three-dimensional model for numerical research of K_{IC}

The three-dimensional FE model for K_{IC} research is presented in Fig. 2.13. The dimensions of this model were used the same as for the two-dimensional model. As the geometry and boundary conditions of C(T) specimen are symmetrical, only half of the model was created. The model was meshed using C3D20R elements [6]. These elements are three-dimensional, brick-shape with 20 nodes. The volume around the crack in the two-dimensional model was meshed using a circular pattern, where at the front of the crack singular elements were used.
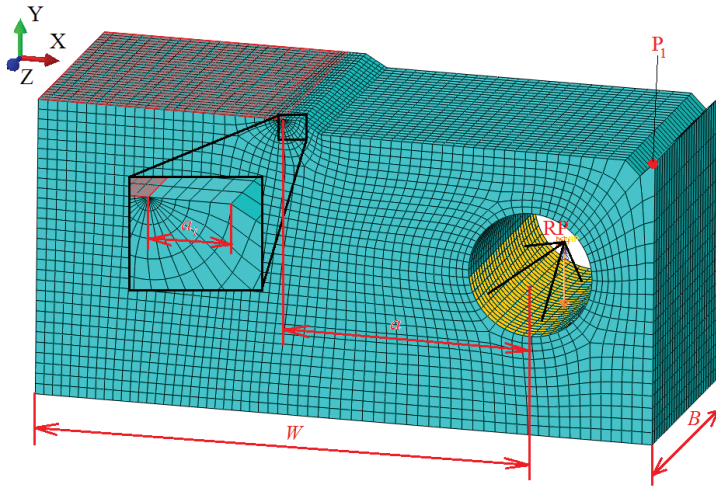
Fig. 2.13. Mesh and boundary conditions of three-dimensional C(T) specimen model for the research of K_{IC}

The calculations were performed using material properties of as-received and the aged steel P91up to 4150 and 11000 hours. The engineering stress-strain curves of these materials are presented in Fig. 2.14. In all cases, the Poison's ratio $\upsilon = 0.3$ was used.
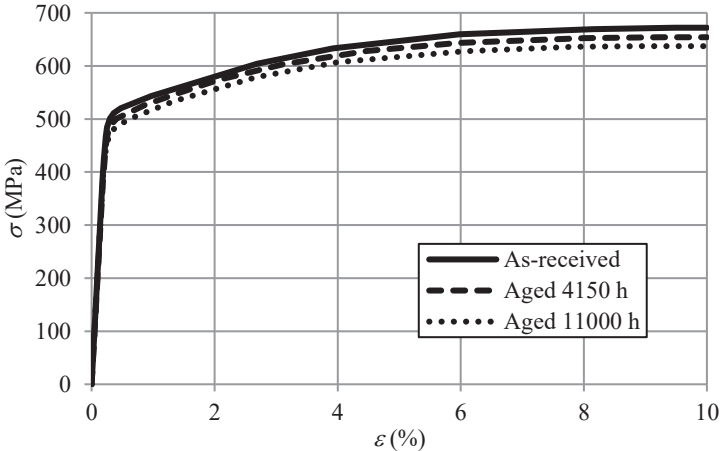
Fig. 2.14. Engineering stress-strain curve of as-received and aged steel P91

Boundary conditions were applied to the P point and symmetry plane marked in red colour (Fig. 2.13). Displacement of the RP point is constrained

27

along X and Z coordinates. Additionally, the rotation of the RP point around Y-axis was also constrained. The displacement of the RP point in the negative direction of the Y-coordinate axis was used as the load. The RP point is connected to one half of the cylindrical hole (yellow colour surface in Fig. 2.13) using rigid coupling elements. To evaluate large deformations and displacements, the nonlinear geometric effect option Nlgeom [6] was activated.

The following results were obtained from the calculations: reaction force, measured at the RP point, stress intensity factor at the crack front, crack opening displacement v. v was determined by tracking the displacements of the point P1 (Fig. 2.13) in the Y-coordinate axis.

In developing the critical stress intensity factor numerical determination method it was not possible to find K_{IC}, as the condition $P_{max}/P_Q \leq 1.1$ described in the ASTM E399-12e3 standard was not met. This shows, that even the aged steel P91 is still too ductile. Therefore, according to the ASTM E399-12e3 standard, to evaluate the fracture toughness of ductile material critical J-integral value J_{IC} must be found.

2.8. Critical J_{IC} evaluation

As in the case of the determination of K_{IC}, the principle of the critical J-integral J_{IC} numerical evaluation is the numerical simulation of J_{IC} experiment determination. J_{IC} determination was based on the ASTM E1820-15 [14]. Steel P91 was also selected for the development of the numerical J_{IC} determination method. An experimental test for experimental J_{IC} determination of the steel P91 was carried out at the Lithuanian Energy Institute.

2.8.1. Experimental research of mechanical properties and J_{IC} of the steel P91

To develop the numerical J_{IC} determination method the experimental determination of J_{IC} of as-received and aged up to 10008 h (~10000 h) at 600 °C and 10872 h (~11000 h) at 650 °C steel P91 was carried out. For easier comparison of the test results, the ageing time of the steel P91 was converted to an equivalent ageing time of 600 °C according to [12]. This way, ~11000 h ageing at 650 °C coincides with ~70000 h ageing at 600 °C. Experimentally determined [15] properties of the steel P91, recalculated at an equivalent ageing time at 600 °C, are presented in Fig. 2.15.

The results of the experimental J_{IC} test of as-received and aged steel P91 are presented in Table 2.4. The obtained results show that as the equivalent ageing time increases the J_{IC} value of the steel P91 decreases. Comparing as-received steels and steels with an ageing time of ~70000 h the average J_{IC} value decreased by 20 %.
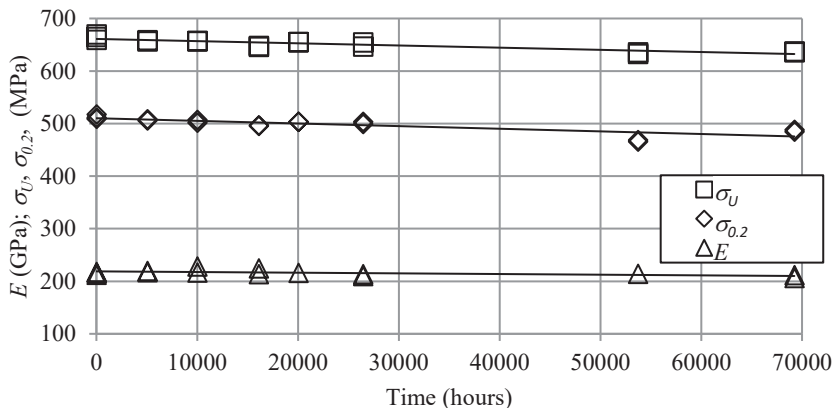
Fig. 2.15. Modulus of elasticity E, yield stress $\sigma_{0.2}$ and ultimate strength σ_U vs. the equivalent ageing time of the steel P91

Table 2.4 Experimentally determined J_{IC} values of as-received and aged steel P91

| Equivalent ageing time, hours	J_{IC}, kN/m
0	509
~10000	475
	394
~70000	432
	379

Experimentally determined as-received and aged steel P91 J-Δa and J-v curves are presented in Section 3.6 together with numerical research results.

2.8.2. Three-dimensional model for numerical research of J_{IC}

The principle of the critical J-integral J_{IC} numerical determination is numerical modelling of the experimental test. Based on the results of K_{IC} numerical research, a three-dimensional C(T) FE model was created for the numerical determination of J_{IC}. The mesh with applied boundary conditions of the created FE model is shown in Fig. 2.16. The geometry and dimensions of the numerical C(T) model correspond to the experimental specimen and meet the ASTM E1820-15 requirements. In all cases, the length of the fatigue crack was a_I=2.8 mm.

The elements and boundary conditions were used the same as for the three-dimensional model used for the determination of K_{IC}. The only differences in this model were the location of the point P1 used for the measurement of the crack opening displacement and the mesh around the crack front. As the C(T) specimen for the determination of J_{IC} has side grooves the geometry becomes more

29

sophisticated and it is not possible to create a mesh using singular elements. Therefore, the volume around the crack front was meshed using the same elements (C3D20R) as for the rest of the model just the size was decreased. To evaluate large deformations and displacements the nonlinear geometric effect option Nlgeom was activated.
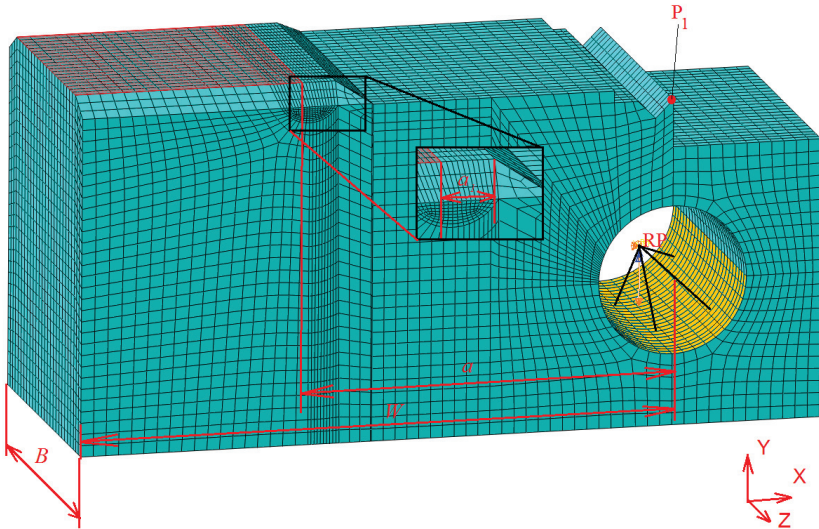

Fig. 2.16. Mesh and boundary conditions of three-dimensional C(T) specimen model for the research of J_{IC}

For the development of the J_{IC} numerical determination method, the C(T) tension test simulations of as-received and aged up to ~10000 h and ~70000 h steel P91 were carried out. To describe the material models the experimentally determined properties shown in Fig. 2.15 and stress-strain curves (Fig. 2.17) were used. In all cases, the Poisson's ratio of $\upsilon = 0.3$ was used.

The following results were obtained from the calculations: reaction force, measured at RP point, J-integral J_I at the crack front and the crack opening displacements v.

According to the ASTM E1820-15 standard for critical J-integral determination of J_{IC}, the J-integral J_I vs. the crack extension Δa curve must be constructed. As the crack growth is not modelled in the numerical model, the crack extension cannot be directly measured. Therefore, the crack opening displacement and the load ratio vs. the crack extension curve was used. Sullivan and Crooker [15] presented a methodology where crack opening displacements were used for the determination of the crack extension. The authors suggest using the polynomial function $a/W = f(E, B, v, F)$ and, in the case of a C(T) specimen with side

30

grooves, to replace the specimen thickness B with the nominal specimen thickness B_N. Since the polynomial function will be used in the developed fracture toughness numerical determination method to determine the crack extension, it is proposed to replace the crack length a with the crack extension Δa.
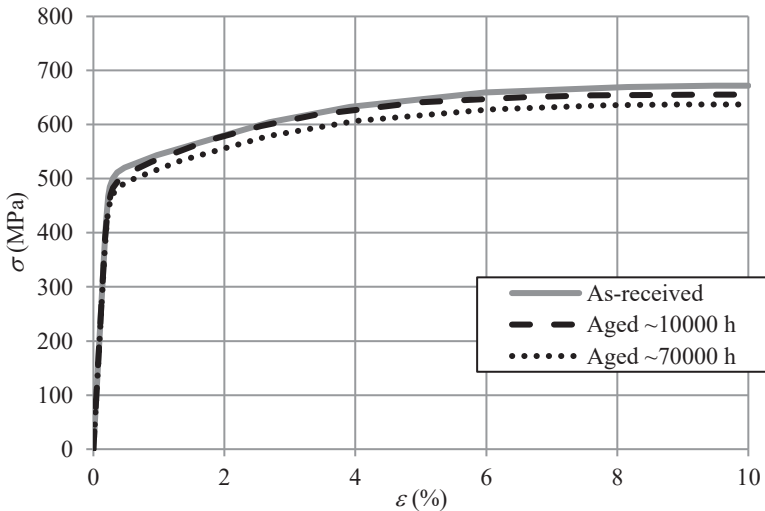
Fig. 2.17. Engineering stress-strain curves of as-received and aged steel P91

The EB_Nv/F vs. $\Delta a/W$ curves used for the determination of the polynomial function later used to predict the crack extensions are described in Section 3.6. The results of the numerical J_{IC} determination and the comparison with experimentally determined critical J-integral values are also presented in this Section.

3. RESEARCH RESULTS AND DISCUSSION

3.1. Results of measurement of hydride size

The measurements of zirconium hydride length and thickness were carried out according to the methodology described in Section 2.2. The measured lengths and thicknesses of zirconium hydride vs. hydrogen concentration are shown in Fig. 3.1.

The measurement of hydride dimensions showed that while the hydrogen concentration increases in zirconium alloy the average length and thickness of the hydride does also increase. Both the hydride length and thickness dependencies on the hydrogen concentration are linear.

The determination of the hydride volume part in the zirconium matrix was carried out according to the procedure described in Section 2.3. Obtained results are shown in Fig. 3.2 and Table 3.1. The measurement results show that the percentage volume part of hydrides on the A-R plane is close to the percentage volume part of the hydride on the R-T plane. This shows that the distribution of hydrides and their geometry (length and thickness) in the A-R and R-T planes are similar, i.e. do not deviate more than 20%.
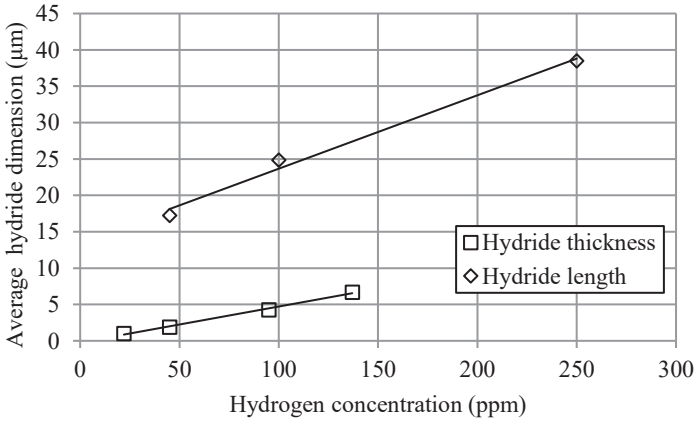
Fig. 3.1. The length and thickness of zirconium hydride vs. hydrogen concentration
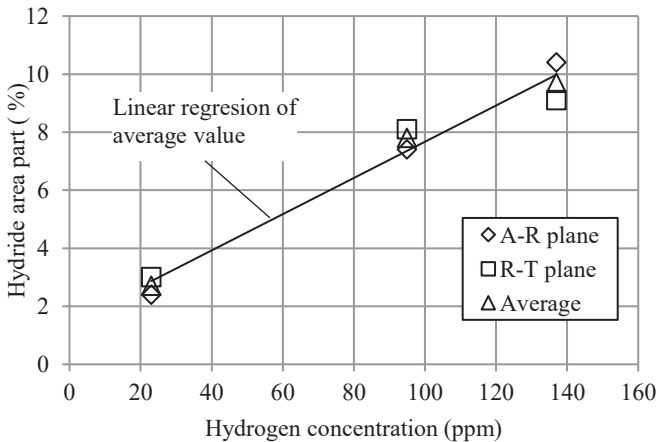
Fig. 3.2. Area part of hydrides vs. hydrogen concentration

According to the stereologic planimetric method (Section 2.3), a determined area part of the hydride can be equated to the volume part, i.e. obtained results

presented in Fig. 3.2 and Table 3.1 correspond to the volume part of the hydride in the zirconium matrix.

Table 3.1. Hydride area part analysis results

Hydrogen concentration, ppm	Area part of hydride, %		Average, %
	A-R plane	R-T plane	
23	2.4	3.0	2.7
84	7.4	8.1	7.8
137	10.4	9.1	9.7
460	32.0	28.6	30.3

3.2. Results of the numerical evaluation of mechanical properties of zirconium alloy with hydrides

The mechanical properties (stress-strain curves) of the zirconium alloy with hydrides were determined using the FE model described in Section 2.4.1. Calculations were made of specimens made of the Zr-2.5Nb FC alloy at hydrogen concentrations of 52, 100, and 140 ppm.

Numerical modelling result (stress-strain curve) for the hydrogen at 140 ppm is shown in Fig. 3.3. In Figure, numerical modelling results are compared with experimentally determined stress-strain curves found in [3] for the hydrogen concentrations of 0 ppm and 140 ppm. It should be noted that experimentally tested specimens found in [3] were saturated with hydrogen and hydrides were formed at the Lithuanian Energy Institute under the same conditions as for the preparation of the microsection samples for the hydride dimensions and volume part measurements.
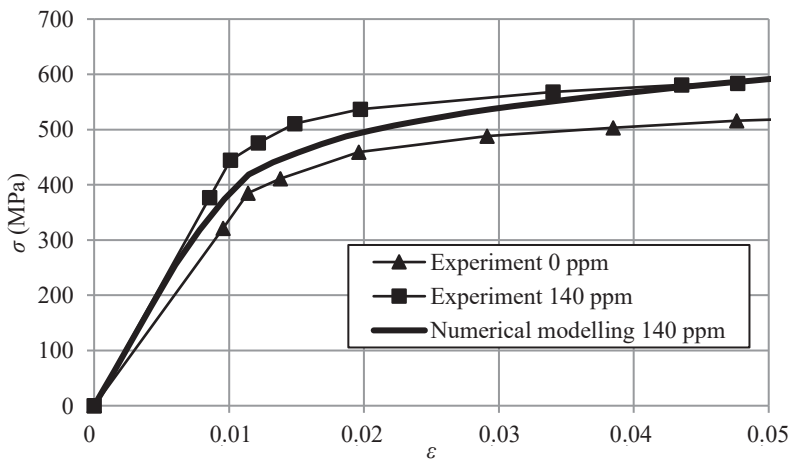
Fig. 3.3. Numerically and experimentally determined stress-strain curves of Zr-2.5Nb alloy

The numerical simulation results in the elastic zone are in good agreement with the experimental data (Fig. 3.3). However, at the beginning of the plastic strain, the numerically determined stresses do deviate from experimentally determined. It should be mentioned too that the numerically determined stress-strain curve has no stress drop, i.e. as the strain increases the stress growth gradually slows down and eventually stops, but the stress does not decrease, what makes the ultimate strength determination impossible.

A comparison of the numerically determined modulus of elasticity with determined experimentally [3] at different hydrogen concentrations is shown in Fig. 3.4. The Figure also shows the linear regression line of the experimental data. The numerical simulation results, as well as the experimental data, show that as the concentration of hydrogen increases, the values of the modulus of elasticity do also increase. This can be explained by the fact that the higher the concentration of hydrogen, the higher the volume part of the hydride, which means that the influence of hydride to the properties of the systems is bigger.
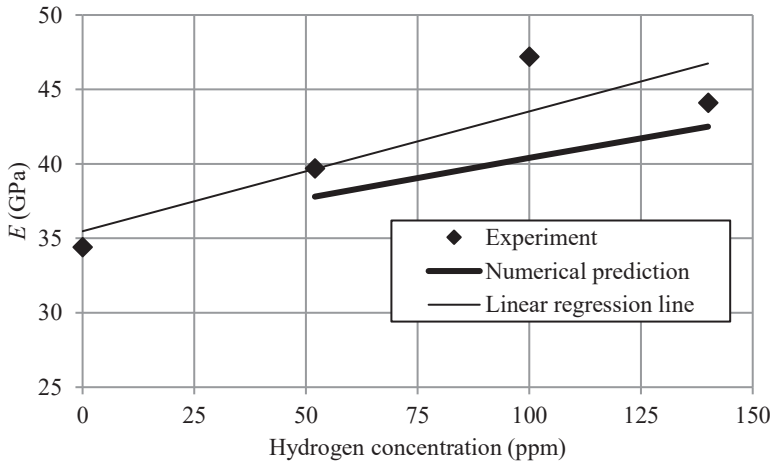
Fig. 3.4. Numerically and experimentally determined modulus of elasticity values vs. hydrogen concentration of Zr-2.5Nb alloy

The comparison of the numerical modelling results with the experimental results of the modulus of elasticity and yield stress of the zirconium alloy with hydrides is shown in Table 3.2. The highest deviation of numerically determined E from the experimental results is up to 9 %. Depending on the hydrogen concentration, the numerically determined yield stress deviates from the experiments in the range of 11–14 %.

Table 3.2. Numerical modelling and experimental [3] results of mechanical properties of Zr-2.5Nb alloy with hydrides

Hydrogen concentration, ppm	E, MPa		Deviation, %	$\sigma_{0.2}$, %		Deviation, %
	Linear regression of experiment	Numerical modelling		Experiment	Numerical modelling	
52	39.7	37.8	4.8	368	418	13.6
100	43.5	40.4	7.1	470	420	10.6
140	46.7	42.5	9.0	470	420	10.6

3.3. Results of the programme ABAQUS validation for the calculation of the fracture parameters

The validation of the fracture mechanics problem solution in the ABAQUS was performed by comparing stress intensity factor K_I values in the internal cracks at the Es-Salam reactor pressure vessel. K_I values were calculated analytically and using the programmes ABAQUS and ANSYS.

The comparison of the stress intensity factor values determined using the programmes ABAQUS and ANSYS and analytical calculations (according to the ASME requirements) in case of axial and circumferential cracks is presented in Fig. 3.5. The Figure shows the calculation results when the ratio of the crack depth and thickness of the reactor pressure vessel wall $a/t = 0.25$. K_I calculations were made at the deepest point of the crack, i.e. when $\Phi = 90°$. According to the figure K_I values calculated using the ABAQUS do very well meet the K_I values calculated analytically. A slightly larger deviation of the ABAQUS results from analytical calculated was obtained when the crack depth and length ratio was equal to $a/c = 1.0$ and reached 7 % and 18 % for axial and circumferential cracks respectively. Comparing the K_I values calculated using the programme ANSYS with analytical calculations obtained a larger deviation than using the programme ABAQUS for both axial and circumferential cracks, except for $a/c = 1.0$. This indicates that the ABAQUS finite element programme calculates the K_I in greater precision than the programme ANSYS, and the resulting accuracy is sufficient for further research. Therefore, it can be stated, that the programme ABAQUS FE is suitable for modelling and numerical research of fracture parameters.
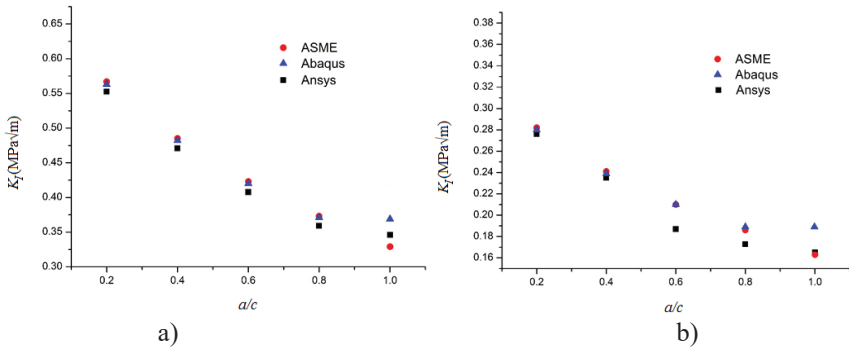
Fig. 3.5. The comparison of K_I values calculated analytically and using the programmes ABAQUS and ANSYS, when $a/t = 0.25$: a) axial crack case; b) circumferential crack case

3.4. Results of research of two-dimensional model used for the numerical determination of K_{IC}

The research of two-dimensional C(T) specimen model, described in Section 2.7.2, was done in the case of the plane strain and plane stress states. The distribution of the equivalent (Mises) stress for both states is shown in Fig. 3.6 a) and b). The results are shown at very small crack opening $v = 0.07$ mm. The best way to see where the stress tends to concentrate is when the load level on the FE model is low. As expected, peak stresses occur at the tip of the crack. Stress fields extend from the edges of the holes where tensile displacements are added to the tip of the crack. This indicates that the FE models are working correctly.
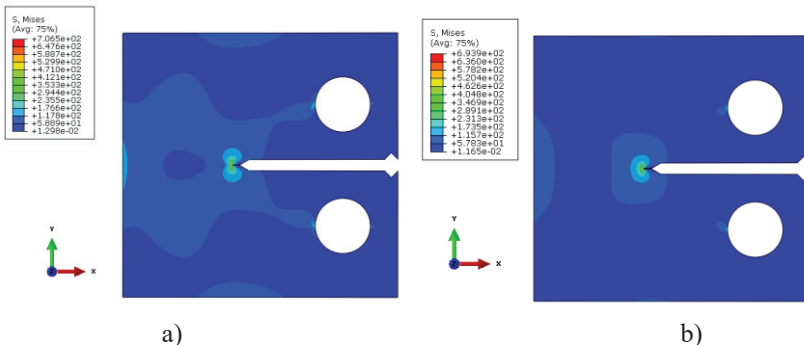

Fig. 3.6. Equivalent (Mises) stress distribution, when crack opening displacement $v = 0.07$ mm: a) plane strain state case; b) plane stress state case

The results of the calculation using the mechanical properties of as-received steel P91 are shown in Fig. 3.7. The Figure shows the dependence of the tensile

force F on the crack opening displacements v determined experimentally and using the two-dimensional numerical FE models. As seen in the Figure, the numerically determined F is higher by 20% in the case of the plane strain state and less than 13% in the case of the plane stress comparing with experimentally determined F at $v = 2.5$ mm. According to the theory of elasticity [16], the plane strain state is applied to the analysis of thick structures where deformations through thickness are not important. In contrast, the plane stress state is used when thin structures are analysed. In the case of C(T) specimen, where biaxial stress state exists, deformations through thickness are important.

Evidently, a two-dimensional numerical model for the standard C(T) specimen of width $W = 50$ mm with a thickness $B = 25$ mm is not suitable. Therefore, the three-dimensional FE model described in Section 2.7.3 was researched. The results of this research are presented in Section 3.5.
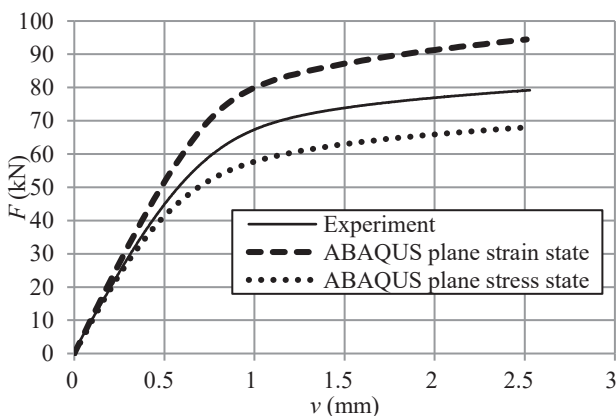
Fig. 3.7. *F* vs. *v* curves determined experimentally and numerically using the two-dimensional FE plane strain and plane stress state models

3.5. Results of the research of the three-dimensional model used for the numerical determination of K_{IC}
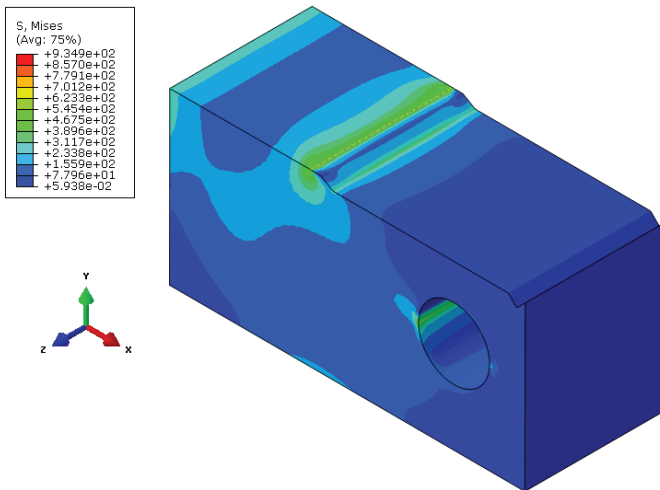
The distribution of equivalent stresses in the three-dimensional C(T) specimen FE model used for the numerical determination of K_{IC} when $v = 0.2$ mm is shown in Fig. 3.8. In terms of two-dimensional models, the peak stresses concentrate at the front of the crack and the stress fields are distributed smoothly from the load application surface to the crack front. This indicates that the loading and boundary conditions have been applied properly and the model is operating correctly.

As described in the ASTM E399-12e3 standard [11], first of all, the determination of the critical stress intensity factor requires the dependence of the

tensile force F on the crack opening displacements v to be constructed. For this purpose, a non-linear numerical analysis of the C(T) specimen was performed. Experimentally and numerically determined F vs. v curves of as-received steel P91 are shown in Fig. 3.9. As seen numerically determined F-v curve is in good agreement with the experimental curves, as the maximum deviation does not exceed 5%.

According to the ASTM E399-12e3 standard, F-v curve is used for the determination of the conditional load P_Q and maximum load P_{max}. The determination of P_Q load for as-received steel P91 is shown in Fig. 3.10.

Using the load P_Q the conditional stress intensity factor K_Q can be found. K_Q can be calculated analytically using the equations described in the ASTM E399-12e3 standard or numerically, using the same C(T) FE model, created in the programme ABAQUS as it has built-in procedures for the calculation of the stress intensity factor K_I values at the crack front. To check the K_I calculation accuracy by the ABAQUS the dependencies of K_I on F determined analytically and numerically are shown in Fig. 3.11. As seen, the numerically constructed line is in good agreement with the line constructed using analytical calculation and the deviation is only 2% at $F = 50$ kN. The deviation occurs due to the fact that, analytically, the determinations of K_I evaluate the plane strain state where deformations along the sample thickness are neglected. However, the three-dimensional FE model does estimate strains and stresses in all three directions.

Fig. 3.8. The distribution of the equivalent (Mises) stress in the three-dimensional FE model when the crack opening displacement $v = 0.2$ mm
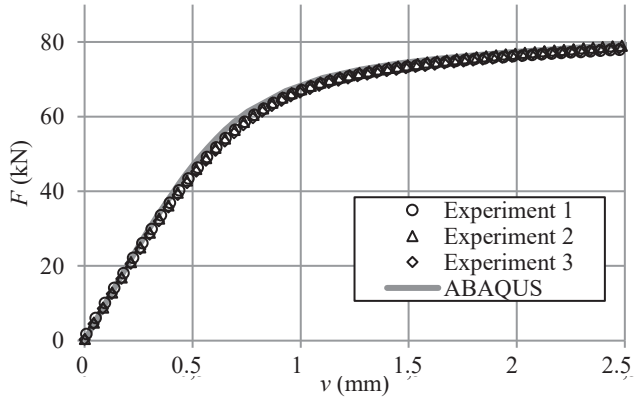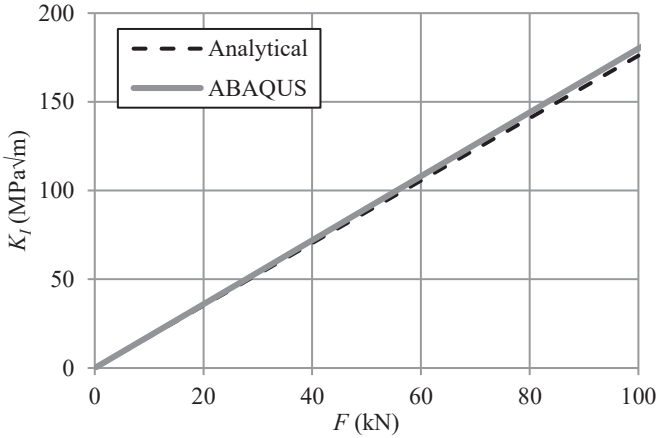
Fig. 3.9. F vs. v curves determined experimentally and numerically using the three-dimensional FE model
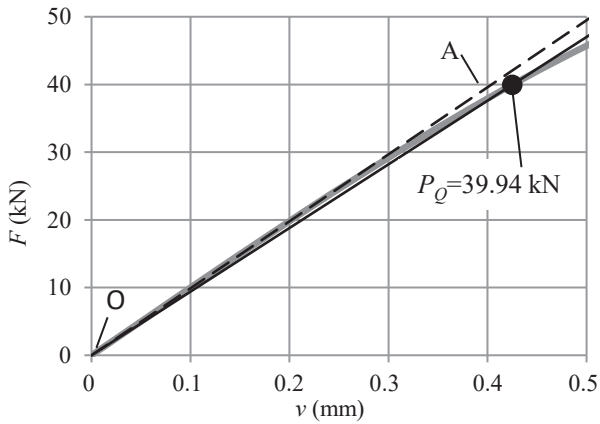
**Fig. 3.10.** Determination of the load P_Q

Fig. 3.11. K_I vs. F determined analytically and numerically using the programme ABAQUS

Based on these findings, further K_Q and K_{max} values will be determined using K_I-F curve constructed by the ABAQUS calculations.

A comparison of numerically determined P_Q and P_{max} loads of as-received and aged steel P91 determined experimentally is shown in Fig. 3.12. The ageing effect in numerical calculations was evaluated by using the material properties of the aged steel P91. The Figure shows that the numerically determined P_Q loads are smaller and P_{max} loads are higher than those obtained experimentally. However, the difference is not significant. The maximum deviation of 9 % was obtained of P_Q load at the ageing time of 11000 h.
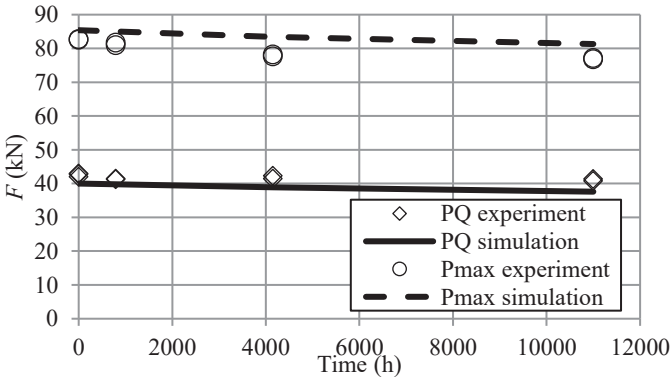
Fig. 3.12. Experimentally and numerically determined P_Q and P_{max} loads at the different ageing time of steel P91

Analogical results were obtained for K_Q and K_{max} numerical determination (Fig. 3.13). As in the case of the P_Q load determination, the numerically determined values of K_Q are lower than experimentally determined and K_{max} values are higher. However, the difference between experimental and numerical results is not significant, with the same deviation of 9 %. The decrease in the stress intensity factor values after ageing of 11000 h is not significant compared to the as-received sample. Experimentally determined K_Q and K_{max} values decreased by 4 % and 7 % and numerically by 6 % and 5 % respectively.
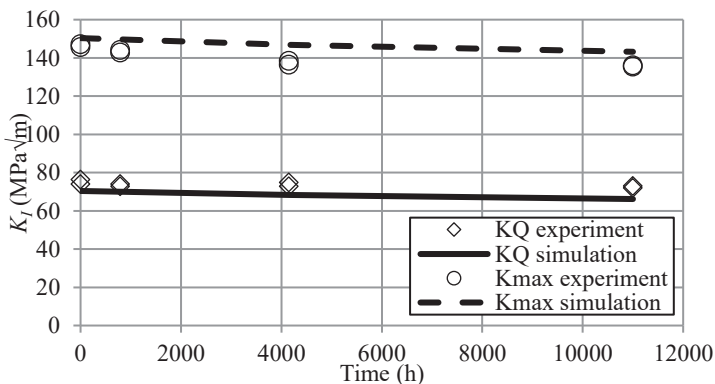
Fig. 3.13. Experimentally and numerically determined K_Q and K_{max} factors at the different ageing time of the steel P91

The conditions described in the requirements of the ASTM E399-12e3 [11] have been checked to equate the conditional stress intensity factor values to the critical stress intensity factor $K_Q = K_{IC}$. As the condition $P_{max}/P_Q \le 1.1$ was not met in all as-received and aged steel P91 cases, therefore $K_Q \ne K_{IC}$. This shows that the steel P91 remains ductile even after relatively long time exposure at high temperatures. In accordance with the ASTM E399-12e3, if the condition $P_{max}/P_Q \le 1.1$ is not met, a critical J-integral should be determined following the ASTM E1820-15 standard [14].

Although the K_{IC} could not be determined for the steel P91, the comparison of the numerical results with experimental data showed good agreement and suitability of the developed numerical methodology for the determination of K_{IC} of brittle materials.

3.6. Results of the research of the three-dimensional model used for the numerical determination of J_{IC}

The results of the research of the three-dimensional C(T) specimen model used for the critical J-integral J_{IC} numerical evaluation are presented in Fig. 3.14 – Fig. 3.17.

Equivalent stress distribution in the FE model of C(T) specimen used for the J_{IC} determination $v = 0.33$ mm is shown in Fig. 3.14. The obtained stress distribution tendencies are the same as for the three-dimensional FE models used for the K_{IC} evaluation. Therefore, it is concluded that the loading and boundary conditions are applied appropriate and the model is working correctly.
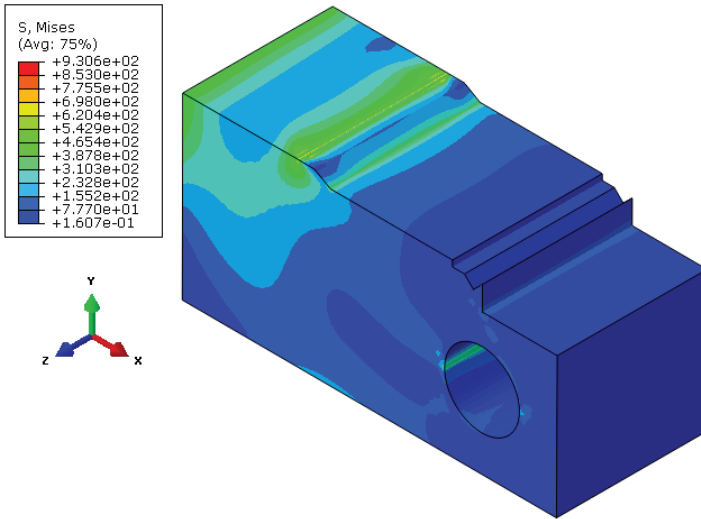

Fig. 3.14. The distribution of the equivalent (Mises) stress in the three-dimensional FE model used for the J_{IC} evaluation when the crack opening displacement $v = 0.33$ mm

Fig. 3.15 shows the numerically and experimentally determined dependencies of the C(T) tensile load F on the crack opening displacement v. The figure shows the results of as-received (a)), aged to ~10000 hours (b)) and aged to ~ 70000 hours (c)) steel P91. As seen, the calculation results do agree well with the experimentally determined curves to the maximum value of the tensile force, i.e. to the top of the curves (maximum deviation recorded at this point do not exceed 4%). However, the drift of the numerical model result from experimentally determined curves starts, where the crack opening displacements v exceed the peak of the F-v curve, i.e. when the force starts to decrease on the experimentally determined curves. In the experiment tension load of C(T) specimen decrease due to the extension of the crack. Since the numerical FE model does not model the crack extension, no force drop is detected. It is noted, that, although a direct crack extension is not modelled, the ABAQUS programme implements virtual crack extension estimation algorithms for the J-integral J_I calculations [17].
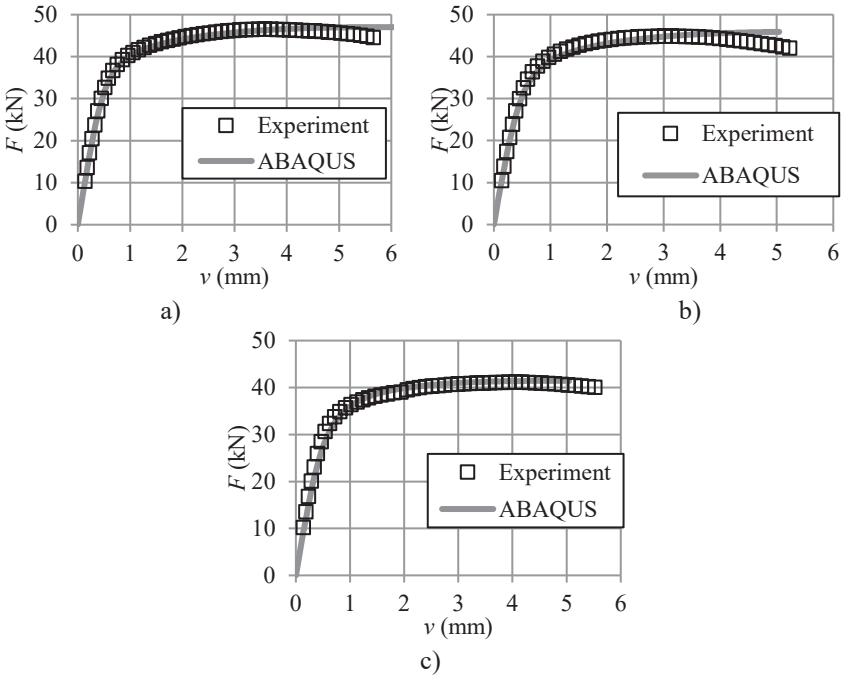
Fig. 3.15. Numerically and experimentally determined C(T) specimen dependencies of the tension load on the crack opening displacement of the steel P91: a) as-received material; b) aged to ~10000 hours; c) aged to~70000 hours

Fig. 3.16 shows the dependencies of $EB_N v/F$ on $\Delta a/W$ of the steel P91. These dependencies were used to find the polynomial function, which is later used for the crack extension evaluation. The polynomial functions were found from the averaged curve derived from the C(T) specimen experimental tension test results of as-received and aged steel P91.
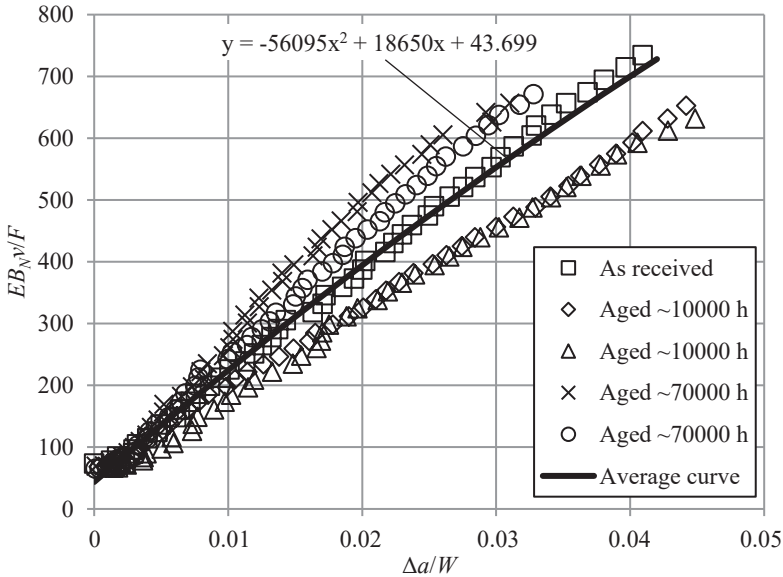
Fig. 3.16. $EB_N v/F$ vs. $\Delta a/W$ of steel P91

Using the average curve shown in Fig. 3.16 the second-order polynomial function was found:

$$\frac{EB_N v}{F} = -56095\left(\frac{\Delta a}{W}\right)^2 + 18650\left(\frac{\Delta a}{W}\right) + 43.699 \,. \qquad (7)$$

J_I value in the crack tip is calculated by the ABAQUS implemented algorithms. Using the three-dimensional FE model the ABAQUS calculates the J_I at all crack front nodes. Therefore, for the numerical evaluation of J_{IC} and the comparison with the experimental data, the average value of the numerically determined J_I over the specimen thickness was used. Having the numerically determined dependencies of F on v (Fig. 3.15) the crack extension Δa from equation (7) can be calculated. Numerically constructed dependencies of J_I on Δa for as-received and aged steel P91 are shown in Fig. 3.17. Numerically constructed curves are compared with the experimentally determined and, in addition, in the case of as-received steel P91 (Fig. 3.17 a) to the curves found in the literature [18]. As seen from the Figure, the numerically determined J_I-Δa curve is in good coincident with the experimentally determined curve up to the crack extension of 0.8 mm. Above 0.8 mm, the curve starts to deviate but still coincide well with the P91-1-C(T)-6 and P91-0.5-C(T)-9 curves found in the literature [18].

Comparison of the numerically determined J_I-Δa curves with experimental curves of aged steel P91 is presented in Fig. 3.17 b and c. In the case of the aged steel P91, ~10000 hours overall good coincidence between the numerical and experimental results was obtained. In the case of the aged up to ~70000 hours, the second half of the curve is slightly more shifted from the experimental results, but most importantly, the first part of the curve, where the 0.2 mm parallel intersects the J_I-Δa curve, coincides well (deviation up to 9 %).

The comparison of the numerically and experimentally determined conditional J-integral values J_Q is presented in Table 3.3. It shows that the numerically determined values of the J-integral in all cases are lower than the mean values of the experimentally determined J_Q. The biggest deviation of the results (11%) was obtained at the ageing of ~70000 h. It should be noted that the critical J-integral is a sensitive characteristic and high scattering of results is a common phenomenon. For example, the J_Q values of the steel P91 found by Konopík and Viehrig [18] studies ranged from 289 kN/m to 523 kN/m.

As the experimental and numerical simulation results have met all the requirements and conditions of the ASTM E1820-15 standard it can be stated that the experimentally and numerically determined $J_Q = J_{IC}$ for as-received and aged steel P91.

The comparison of the numerical simulation results with the experimental data presented in this section confirms that the J_{IC} numerical evaluation method is suitable for the fracture toughness determination of ductile materials.

The application of the developed numerical method for determination of the fracture toughness of the Zr-2.5Nb alloy with hydrides is presented in the next section of the dissertation.
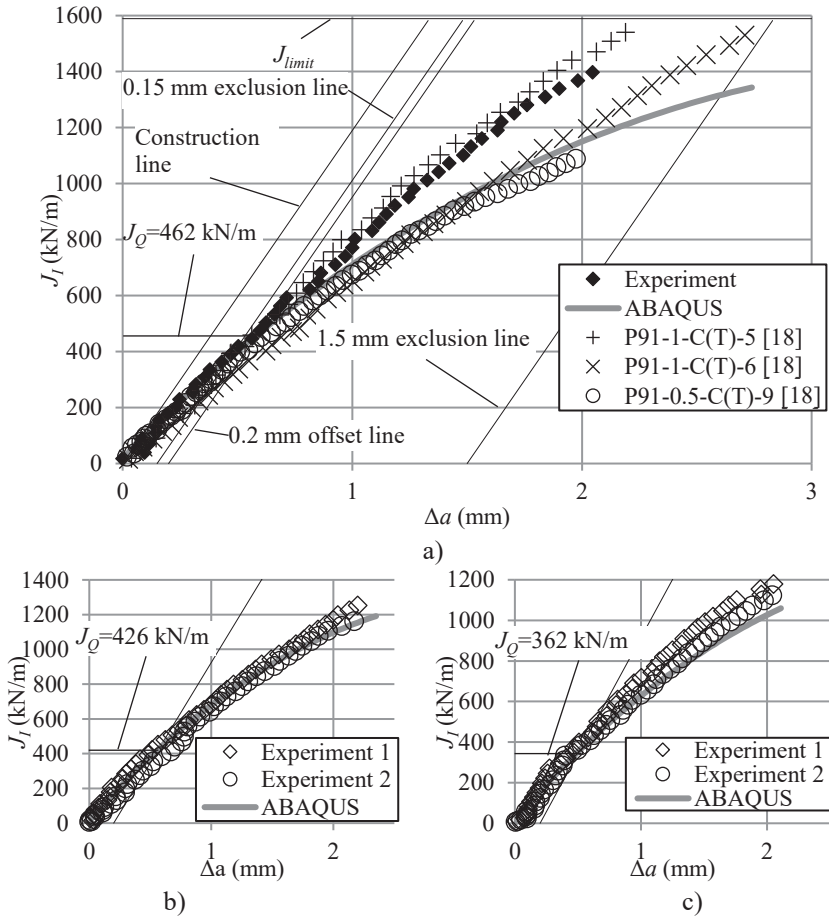
Fig. 3.17. Experimentally and numerically determined J_I-Δa curves of the steel P91:
a) as-received; b) aged to ~10000 hours; c) aged to ~70000 hours

Table 3.3. Numerically and experimentally determined J_Q values of the steel P91

Equivalent ageing time, hours	J_Q, kN/m			Deviation, %
	Experiment	Average	Numerical modelling	
0	509	509	462	9
~10000	475	434.5	426	2
	394			
~70000	432	405.5	362	11
	379			

4. APPLICATION OF THE DEVELOPED NUMERICAL METHOD FOR THE DETERMINATION OF FRACTURE TOUGHNESS OF ZR-2.5NB ALLOY WITH HYDRIDES

The demonstration of the application and obtained results of a developed numerical method for the determination of fracture toughness of zirconium alloy with hydrides are presented in this section of the dissertation. According to the developed numerical method to evaluate fracture toughness the determination of the critical stress intensity factors and critical J-integrals of Zr-2.5Nb TMT-2 FC alloy saturated with hydrogen was carried out. The results of the numerical study were compared with the experimental data [3].

4.1. Evaluation of the critical stress intensity factor of the Zr-2.5Nb TMT-2 alloy saturated with hydrogen

The Zr-2.5Nb alloy of Ignalina NPP FC saturated with hydrogen was chosen for the numerical determination of critical stress intensity factor. Numerical studies were performed at 0, 52, 100, and 140 ppm hydrogen concentrations. Mechanical properties of the zirconium alloy with different hydrogen concentrations presented in Section 3.2 were used to describe the material behaviour.

To compare not only the numerically determined K_{IC} but also the selected conditional tensile load P_Q with the experimental results, a FE model of the C(T) specimen was created, the dimensions of which coincide with those of the experimental specimen [3]. FE model mesh and boundary conditions are shown in Fig. 4.1. As the specimen for experimental studies was made of Ignalina NPP FC tube with an internal diameter of 79.5 mm and a wall thickness of ~4 mm the relatively small specimens of $W = 17$ mm, $B = 4.2$ mm, $a = 6.75$ mm, and $a_1 = 1.8$ mm were machined. The FE model was meshed using C3D20R elements. The volume around the crack was meshed using a circular pattern and the singular elements were selected at the front of the crack. To evaluate large deformations and displacements the nonlinear geometric effect option (Nlgeom) was activated. The boundary conditions were used the same as for the model described in Section 2.7.3.

F-v dependencies were obtained by nonlinear calculations which estimate elastic-plastic properties of the material. Conditional tension loads P_Q were determined for the Zr-2.5Nb TMT-2 FC alloys without hydrogen and with hydrogen concentration of 52, 100, and 140 ppm. The numerically determined loads P_Q at different hydrogen concentrations are shown in Fig. 4.2. The Figure also shows experimentally determined load P_Q (diamond-shaped points) and their mean values (dotted line). The numerical values are in good agreement with the experimental data, with a tolerance of 3%.
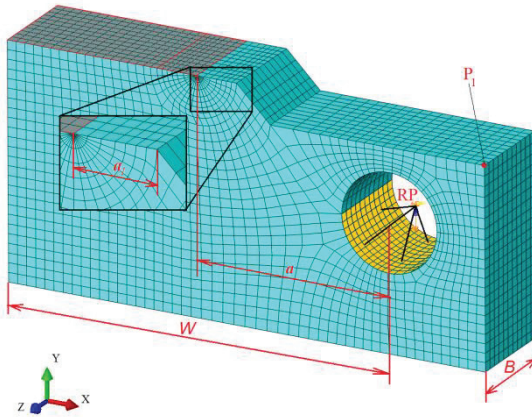
Fig. 4.1. FE mesh and boundary conditions of C(T) specimen model used for the K_{IC} evaluation of the Zr-2.5Nb TMT-2 alloy
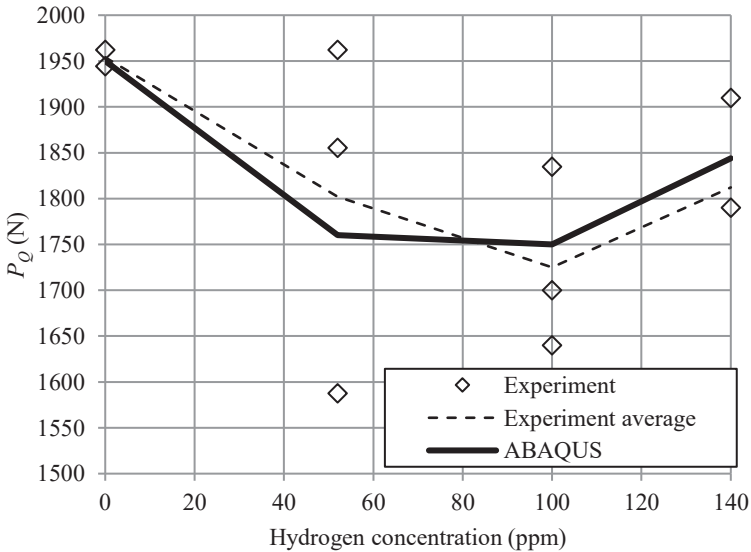
Fig. 4.2. Numerically and experimentally [3] determined P_Q load of zirconium alloy at a different hydrogen concentration

A comparison of numerically and experimentally determined K_Q values is presented in Fig. 4.3. All numerically determined K_Q values are higher than the average experimentally determined values, but the difference is not significant and

48

does not exceed 11 %. Also, the shape of the numerically determined K_Q values trend corresponds to the experimental data; as the hydrogen concentration increases from 0 ppm to 100 ppm the numerically determined K_Q decreases by 2.99 MPa√m and experimentally by 4.5 MPa√m, which is 8 % and 13 %, respectively. Over hydrogen concentration of 100 ppm, the K_Q values slightly increase.
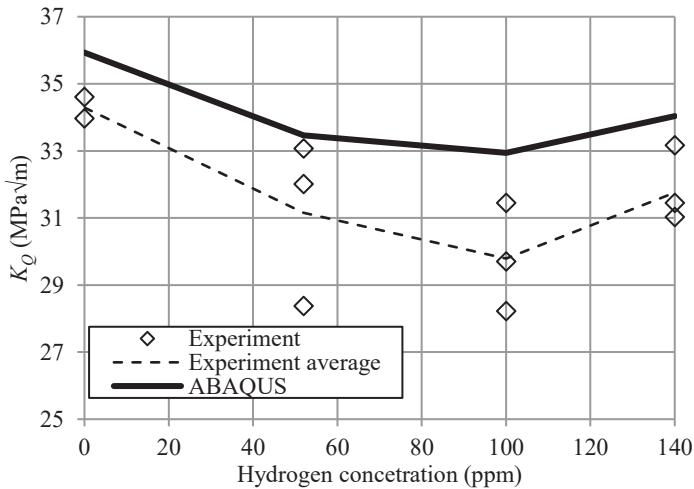
Fig. 4.3. Numerically and experimentally [3] determined the K_Q factor of zirconium alloy at a different hydrogen concentration

Checking the K_{IC} evaluation results with the requirements of the ASTM E399-12e3 [11] not all conditions were met. Therefore, $K_Q = K_{IC}$, which means that the critical J-integral value J_{IC} needs to be found in order to evaluate the fracture toughness of the Zr-2.5Nb TMTO-2 alloy at 0-140 ppm hydrogen concentration.

4.2. Evaluation of the critical J-integral of the Zr-2.5Nb TMT-2 alloy saturated with hydrogen

Numerical evaluation of the critical J-integral J_{IC} of the Zr-2.5Nb TMT-2 alloy with hydrides was performed according to the methodology presented in Section 2.8. Numerical studies were performed at hydrogen concentrations of 0, 52, 100, and 140 ppm. Mechanical properties of zirconium alloy with different hydrogen concentrations presented in Section 3.2 were used to describe the material behaviour. The numerically determined J_{IC} values were compared with experimentally determined values in [3].

The same FE model was used for the numerical determination of J_{IC} as for K_{IC} determination (Section 4.1, Fig. 4.1). The only differences were that the fatigue crack length $a_1 = 2.2$ mm and the crack opening displacements were measured at the load application point RP.

The numerical simulation results of C(T) specimen tension tests are shown in Fig. 4.4. The obtained results were compared with the experimental data. As seen at low values of v a good agreement of numerical results with experimental data was obtained in all cases. Although for zirconium alloys with hydrides the numerical results do separate from experimental data when v values are above the peaks of the experimental curves, the numerically determined maximum tensile forces F are still close to the experimentally determined values and the deviation does not exceed 5 %.

As described in Section 2.8.2, a polynomial function for the crack extension determination is required to construct the J_I-Δa curve. The results of experimental studies of the Zr-2.5Nb TMT-2 alloy without hydrogen were used to find the polynomial function and the generated dependencies of EBv/F on $\Delta a/W$ are presented in Fig. 4.5.

Second-order polynomial expression determined from average curve:

$$\frac{EBv}{F} = 15719 \left(\frac{\Delta a}{W}\right)^2 + 2401.5 \left(\frac{\Delta a}{W}\right) + 45.155 . \qquad (8)$$

To find the J_Q the J_I-Δa curves were constructed using the equation (8) and the calculation results of the 3D FE model. An example of a numerically constructed J_I-Δa curve for Zr-2.5Nb TMT-2 alloy without a hydrogen is shown in Fig. 4.6. The numerically constructed curve is between the experimental curves and the crack extension $\Delta a = 1.2$ mm, which indicates a good agreement with experimental data. At the intersection of the J_I-Δa curve and 0.2 mm offset line, $J_Q = 104$ kN/m was found.
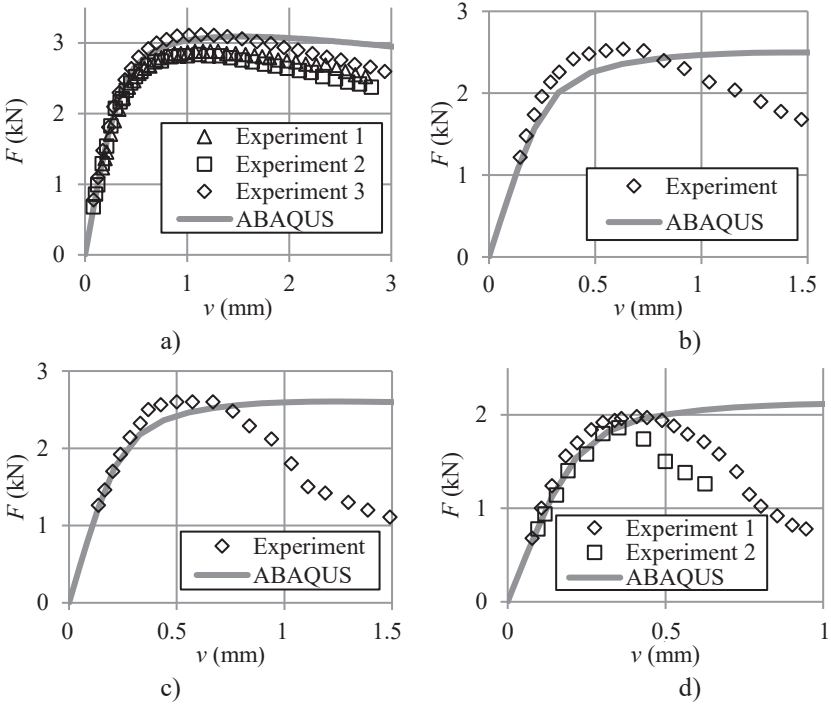
Fig. 4.4. Numerically and experimentally [3] determined F-v curves at a different hydrogen concentration: a) 0 ppm; b) 52 ppm; c) 100 ppm; d) 140 ppm
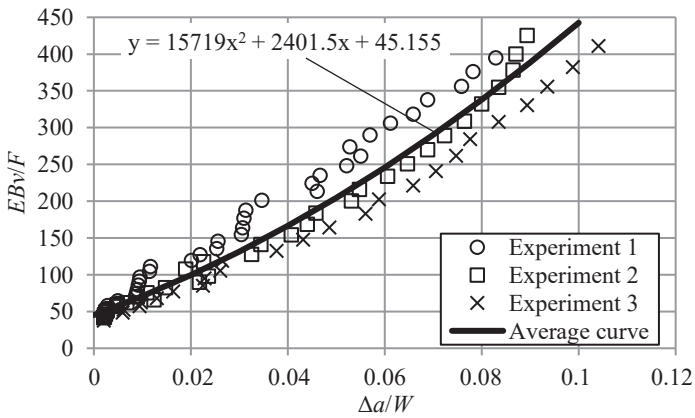
Fig. 4.5. EBv/F vs. $\Delta a/W$ of Zr-2.5Nb alloy without hydrogen
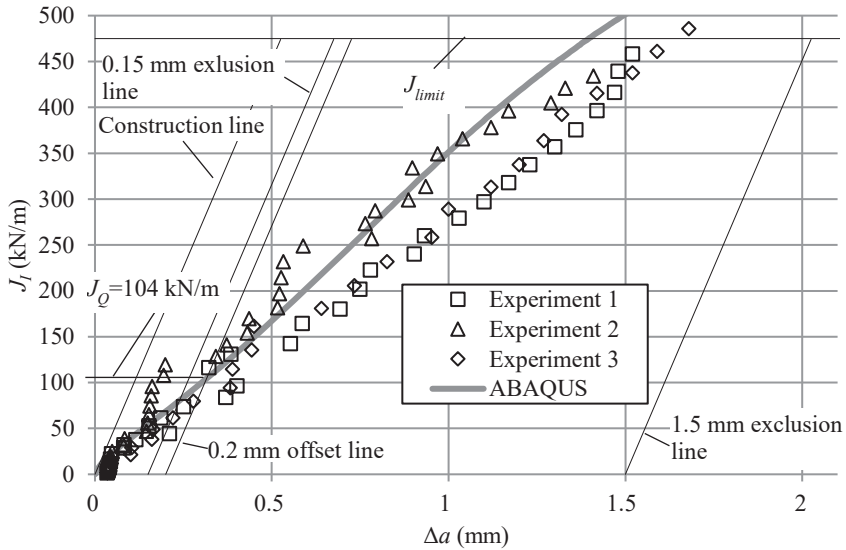
Fig. 4.6. Numerically and experimentally [3] determined J_I-Δa curves for the Zr-2.5Nb alloy without hydrogen

As experimental and numerical simulation results have met all the requirements and conditions of the ASTM E1820-15 standard it can be stated that the determined $J_Q = J_{IC}$ for the Zr-2.5Nb TMT-2 alloy with and without hydrides.

The dependence of the numerically and experimentally determined J_{IC} on hydrogen concentration is shown in Fig. 4.7. The numerically determined values of J_{IC} do decrease by 68 % (from 104 kN/m to 33 kN/m) and experimentally by 84% (from 95 kN/m to 15 kN/m) while hydrogen concentration increases from 0 ppm to 140 ppm. The numerical results are in good agreement with the experimental results until the hydrogen concentration reaches 52 ppm. Over 52 ppm, the deviation of the numerical results from experimentally obtained results rises as the concentration of hydrogen continues to increase.

The numerically and experimentally determined J_{IC} values at different hydrogen concentrations are shown in Fig. 4.7.
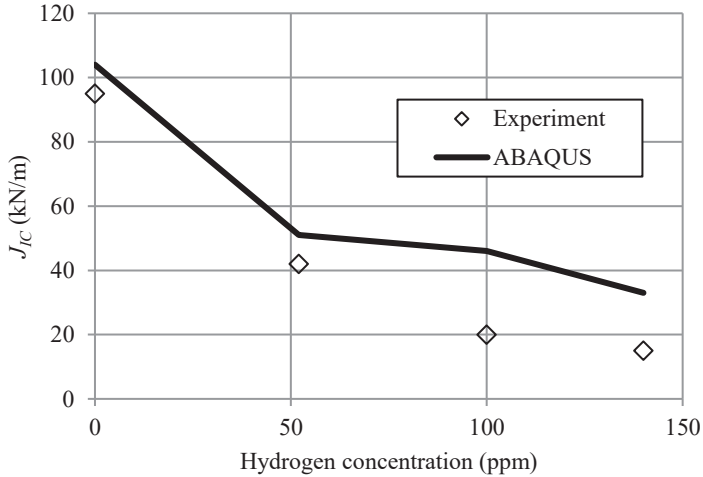
Fig. 4.7. Numerically and experimentally [3] determined J_{IC} values at a different hydrogen concentration

Using the developed numerical evaluation method and determined polynomial function (8) it is recommended to estimate the fraction toughness of the Zr-2.5Nb TMT-2 alloy up to hydrogen concentration limit of 52 ppm. This threshold is sufficient for the FC assessment since the RBMK type reactors FC have an average of 52 ppm after 30 years of operation [19]. The accuracy of numerical evaluation must be increased to estimate the fracture toughness above hydrogen concentration of 52 ppm. This can be done by carrying out a larger number of experimental tests on zirconium alloy, which allows determining polynomial function for the determination of the crack extension more accurately.

CONCLUSIONS

After conducting the numerical research of the fracture toughness of nuclear energy objects construction elements and experimental measurements of zirconium hydride dimensions the following conclusions were made:

1. Hydrides in a fuel channel tube made of the Zr-2.5Nb TMT-2 alloy tend to form in the circumferential-axial direction of the tube. The measurements of hydrides showed that as the hydrogen concentration increases the average thickness, the length and volume part of hydrides in the zirconium matrix do also increase, and their dependencies on hydrogen concentration can be described by a linear function.

2. The developed numerical method allows determining the modulus of the elasticity of zirconium alloy with hydrides by comparing with experimental data with 9% error and yield strength with 14% error.

3. The two-dimensional finite element model using standard compact tension specimens is not suitable for the determination of critical fracture toughness value of the material since the P_Q value does deviate from experimental results up to 15% for the plane strain states and up to 47% for the plane stress states. However, the determined P_Q values using the three-dimensional finite element model do deviate from experimental results only up to 5%. The determined critical stress intensity factor values of zirconium alloys with hydrides using the three-dimensional finite element model of compact tension specimen do not deviate more than 10% from the experimental data.

4. Using the determined second-order polynomial equation, it is possible to estimate the crack growth in the compact tension specimen. The numerically determined crack growth is up to 10% higher than obtained experimentally.

5. The critical J-integral values of zirconium alloy with hydrides determined numerically are higher than determined experimentally up to 20% when the hydrogen concentration in the alloy is less than 52 ppm. As the concentration of hydrogen increases the error of numerical determination does also increase. Therefore, it is recommended to use the developed numerical evaluation method and determined polynomial function to evaluate the degradation resistance of the Zr-2.5Nb TMT-2 alloy up to the hydrogen concentration limit of 52 ppm.

REFERENCES

1. KEARNS, J. J. Terminal solubility and partitioning of hydrogen in the alpha phase of zirconium, Zircaloy-2 and Zircaloy-4. *Journal of Nuclear Materials*. 1967, vol. 22(3), pp. 292-303.
2. CRANK J. *Mathematics of diffusion*. Oxford, 1979.
3. DAUNYS, M., DUNDULIS, R., GRYBENAS, A. and KRASAUSKAS, P. Hydrogen influence on mechanical and fracture mechanics characteristics of zirconium Zr–2.5Nb alloy at ambient and elevated temperatures. *Nuclear Engineering and Design*. 2008, vol. 238(10), pp. 2536–2545. Available from: https://linkinghub.elsevier.com/retrieve/pii/S0029549308002781
4. VARIAS, A.G. and MASSIH, A.R. Temperature and constraint effects on hydride fracture in zirconium alloys. *Engineering Fracture Mechanics*. 2000, vol. 65(1), p. 29–54. Available from: https://linkinghub.elsevier.com/retrieve/pii/S0013794499001071
5. ANDERSON, T L. *Fracture Mechanics: Fundamentals and Applications, Fourth Edition*. CRC Press, 2017. ISBN 9780849316562.
6. ABAQUS/CAE User's Manual, Version 6.11. 2011.
7. IEEE Standard for System and Software Verification and Validation. 2012. Available from: https:/doi.org/10.1109/IEEESTD.2012.6204026
8. *ANSYS Mechanical APDL Fracture Analysis Guide 17.0*. 2016. Southpointe, 2600 ANSYS Drive, Canonsburg, PA 15317 : ANSYS Inc. 17.0.
9. ASME Boiler and Pressure Vessel Code. *Section XI - Rules for inservice inspection of nuclear power plant components*. ASME, 2004.
10. SAAD, D., DUNDULIS, G. and JANULIONIS, R. Numerical simulation of SIF in Es-Salam research reactor vessel. *Engineering Failure Analysis*. 2019. Vol. 96. pp. 394-408. Prieiga per: https://doi.org/10.1016/j.engfailanal.2018.10.014
11. ASTM E399-12. Standard Test Method for Linear-Elastic Plane-Strain Fracture Toughness KIc of Metallic Materials. 2013.
12. GRYBĖNAS, A., MAKAREVIČIUS, V., BALTUŠNIKAS, A., LUKOŠIŪTĖ, I. and KRIŪKIENĖ, R. Correlation between structural changes of M23C6 carbide and mechanical behaviour of P91 steel after thermal aging. *Materials Science and Engineering: A*. 2017, vol. 696, pp. 453–460. Available from: https://linkinghub.elsevier.com/retrieve/pii/S0921509317305804
13. BS EN 10002-1:2001 / ISO 6892-1. *Metallic materials - Tensile testing - Part 1: Method of test at room temperature.* 2009.
14. ASTM E1820-15A. Standard Test Method for Measurement of Fracture Toughness. 2015.
15. SULLIVAN, A.M. and CROOKER, T.W. A crack-opening-displacement technique for crack length measurement in fatigue crack growth rate testing—

development and evaluation. *Engineering Fracture Mechanics*. 1977, vol. 9(1), pp. 159–166. Available from: https://linkinghub.elsevier.com/retrieve/pii/0013794477900613

16. MACERI, A. *Theory of Elasticity*. Berlin, Heidelberg : Springer Berlin Heidelberg, 2010. ISBN 978-3-642-11391-8. Available from: http://link.springer.com/10.1007/978-3-642-11392-5

17. ZHU, X.K. and LEIS, B.N. Bending modified J–Q theory and crack-tip constraint quantification. *International Journal of Fracture*. 2006, vol. 141(1–2), pp. 115–134. Available from: http://link.springer.com/10.1007/s10704-006-0068-5

18. KONOPÍK, P. and VIEHRIG, H.W. Fracture Toughness Characterisation Of The Martensitic Chromium Steel P91. *COMAT 2012 2nd International Conference on Recent Trends in Structural Materials*. 2012.pp. 1–10.

19. IAEA. IAEA - TECDOC-997 - Water channel reactor fuels and fuel channels: Design, performance, research and development. Vienna, 1996.

PUBLICATIONS RELATED TO THE DISSERTATION

Articles in the journals referred in *Clarivate Analytics Web of Science Core Collection* database

1. Saad D., Dundulis G., Janulionis R. Numerical simulation of SIF in Es-Salam research reactor vessel. *Engineering Failure Analysis*, 2019, 96, pp. 394-408. ISSN 1350-6307.

Articles in the journals referred to in the international scientific database

1. Janulionis R., Dundulis G., Kriūkienė R., Grybėnas A. Numerical prediction of mechanical properties of zirconium alloy with hydrides using finite element method. *Energetika*, 2018, 64 (1), pp. 43-51. ISSN 0235-7208

Publications at the international conferences

1. Dundulis G., Janulionis R., Makarevičius V., Grybėnas A. Fracture toughness numerical modelling of the martensitic chromium steel. *25th Anniversary International Conference on Metallurgy and Materials (METAL 2016)*, May 25–27, 2016, Brno, Czech Republic, EU. ISBN 978-80-87294-67-3.
2. Janulionis R., Dundulis G., Grybėnas A. Numerical investigation of critical stress intensity factor. *The 13th International Conference of Young Scientists on Energy Issues (CYSENI 2016)*, May 26–27, 2016, Kaunas, Lithuania, pp. 226–233. ISSN 1822-7554.
3. Janulionis R. Numerical investigation of J-integral. *The 14th International Conference of Young Scientists on Energy Issues (CYSENI 2017)*, May 25–26, 2017, Kaunas, Lithuania, pp. 335–341. ISSN 1822-7554.
4. Janulionis R., Dundulis G., Grybėnas A. Numerical investigation of hydrogen influence on stress intensity factor of zirconium alloy. *Mechanika 2018: Proceedings of the 23rd International Scientific Conference*, May 18, 2018, Druskininkai, Lithuania, Technologija, 2018, pp. 58–61. ISSN 1822-2951.
5. Janulionis R. Numerical investigation of hydrogen influence on J-integral of zirconium alloy. *The 16th International Conference of Young Scientists on Energy Issues (CYSENI 2019)*, May 23–24, 2019, Kaunas, Lithuania, pp. 234–242. ISSN 1822-7554.

Presentations at the international conferences

1. Dundulis G., Janulionis R., Makarevičius V., Grybėnas A. Fracture toughness numerical modelling of the martensitic chromium steel. *The 25th Anniversary International Conference on Metallurgy and Materials (METAL 2016)*, May 25–27, 2016, Brno, Czech Republic, EU. ISBN 978-80-87294-67-3.
2. Janulionis R., Dundulis G., Grybėnas A. Numerical investigation of critical stress intensity factor. *The 13th International Conference of Young Scientists on Energy Issues (CYSENI 2016)*, May 26–27, 2016, Kaunas, Lithuania, pp. 226–233. ISSN 1822-7554.
3. Janulionis R. Numerical investigation of J-integral. *The 14th International Conference of Young Scientists on Energy Issues (CYSENI 2017)*, May 25–26, 2017, Kaunas, Lithuania, pp. 335–341. ISSN 1822-7554.
4. Janulionis R., Dundulis G., Grybėnas A. Numerical investigation of hydrogen influence on stress intensity factor of zirconium alloy. *Mechanika 2018: Proceedings of the 23rd International Scientific Conference*, May 18, 2018, Druskininkai, Lithuania, Technologija, 2018, pp. 58–61. ISSN 1822-2951.
5. Janulionis R., Kriūkienė R. Numerical prediction of mechanical properties of zirconium alloy with hydrides using finite element method. *The 15th International Conference of Young Scientists on Energy Issues (CYSENI 2018)*, May 23–25, 2018, Kaunas, Lithuania, pp. 408. ISSN 1822-7554.
6. Janulionis R. Numerical investigation of hydrogen influence on J-integral of zirconium alloy. *The 16th International Conference of Young Scientists on Energy Issues (CYSENI 2019)*, May 23–24, 2019, Kaunas, Lithuania, pp. 234–242. ISSN 1822-7554.

About the author

Name: Remigijus

Surname: Janulionis

Date of birth: 13 July 1982

Place of birth: Kaunas, Lithuania

E-mail: Remigijus.Janulionis@lei.lt

Education:

1988–2000 – Kaunas *Veršvų* secondary school;

2000–2004 – Kaunas University of Technology, Bachelor in Mechanical Engineering;

2004–2006 – Kaunas University of Technology, Master in Mechanical Engineering;

2015–2019 – the Lithuanian Energy Institute, PhD studies in Technological Sciences, Energetics and Power Engineering.

REZIUMĖ

Ši disertacija skirta hidridų ir terminio poveikio įtakos branduolinės energetikos objektų konstrukcinių elementų irimui skaitiniam tyrimui.

Branduolinių elektrinių kuro apvalkalai yra gaminami iš cirkonio lydinio, jie be kitiems metalams būdingų senėjimo mechanizmų taip pat yra veikiami vandenilio absorbcijos ir jį lydinčio lėtinio hidridinio pleišėjimo mechanizmų. Apvalkaluose esantis branduolinis kuras po eksploatacijos yra saugomas panaudoto kuro baseinuose, trumpalaikio saugojimo konteineriuose, vėliau laidojamas giluminiuose atliekynuose. Visais atvejais yra svarbus kuro apvalkalo patikimumas, turi būti užtikrinamas jo struktūrinis vientisumas bei sandarumas.

Medžiagų senėjimo poveikis įprastai vertinamas eksperimentiniais bandymais laboratorijoje. Kuro apvalkalai yra apsaugos priemonė, neleidžianti radioaktyviems skilimo produktams pasklisti į aplinką, jų eksperimentiniai tyrimai yra sudėtingi ir brangūs, todėl reikalingi alternatyvūs medžiagos senėjimo įvertinimo metodai.

Kanalinio tipo reaktorių kuro kanalai, kaip ir kuro apvalkalai, pagaminti iš cirkonio lydinio, todėl ir juos veikia tokie patys senėjimo mechanizmai. Senėjimo mechanizmai turi ženklią įtaką kuro kanalų ir viso reaktoriaus patikimumui.

Skaitinės metodikos sukūrimui buvo tirti dvimačiai ir trimačiai baigtinių elementų modeliai. Skaitinis standartinių kompaktinių tempimo bandinių tyrimas parodė, kad dvimačiai baigtinių elementų modeliai tiek taikant plokščią deformacijų būvį, tiek ir plokščią įtempių būvį, nėra tinkami irimo tąsumui įvertinti. Tyrimuose pademonstruota, jog šiam tikslui geriau tinka trimatis baigtinių elementų kompaktinio tempimo bandinio modelis.

Nagrinėjant irimo tąsumo parametrus, tyrimai atskleidė, kad net ir esant santykinai didelei vandenilio koncentracijai – 140 ppm, TMO-2 Zr-2,5Nb lydinys išlieka gana plastiškas, todėl nustatomas tik sąlyginis įtempių intensyvumo koeficientas K_Q. Todėl, norint įvertinti šio lydinio irimo tąsumą, reikia rasti kritinę J-integralo J_{IC} vertę.

Atliekant minėtus tyrimus, parengta skaitinio modeliavimo metodika leidžianti įvertinti cirkonio lydinio mechanines savybes ir irimo tąsumą priklausomai nuo vandenilio koncentracijos.

Pagrindinis disertacijos tikslas – naudojant sukurtą metodiką nustatyti branduolinės energetikos objektų konstrukcinių elementų, pagamintų iš cirkonio lydinių, irimo tąsumą įvertinant vandenilio absorbcijos mechanizmą ir terminį poveikį.

Norint pasiekti užsibrėžtą tikslą reikia išspręsti toliau nurodytus uždavinius:
1. Eksperimentiškai išmatuoti cirkonio hidridų matmenis priklausomai nuo vandenilio koncentracijos.
2. Sukurti skaitinio modeliavimo metodą ir jį naudojant ištirti cirkonio lydinio su hidridais mechanines charakteristikas;

3. Sukurti skaitinio modeliavimo metodą ir jį naudojant nustatyti cirkonio lydinio su hidridais kritinę įtempių intensyvumo koeficiento vertę.

4. Sukurti skaitinio modeliavimo metodą, leidžiantį nustatyti plyšio pailgėjimą kompaktiniame bandinyje.

5. Sukurti skaitinio modeliavimo metodą ir jį naudojant nustatyti cirkonio lydinio su hidridais kritinę J-integralo vertę.

Išsprendus disertacijoje suformuotus uždavinius sukurta nauja skaitinio modeliavimo metodika, leidžianti skaitiniais metodais nustatyti cirkonio lydinių irimo tąsumą esant skirtingoms vandenilio koncentracijoms. Plyšio pailgėjimo nustatymo metodai papildyti pasiūlyta ir validuota daugianare lygtimi.

Sukurta metodika tinkama naudoti įvairių metalo lydinių įtempių intensyvumo koeficientams bei J-integralo vertėms nustatyti. Taikant šią metodiką branduolinės energetikos objektų konstrukcinių elementų pagamintų iš cirkonio lydinių, t. y. kuro kanalų bei kuro apvalkalų, vertinimui, galima prognozuoti jų savybių pokytį dėl vandenilio absorbcijos mechanizmo eksploatacijos ar branduolinio kuro saugojimo metu. Tai didina visos branduolinės elektrinės patikimumą. Tai labai aktualu panaudoto branduolinio kuro saugojimo metu, kadangi eksploatuojant sukaupti vandenilio koncentracijos kiekiai kuro apvalkale yra dideli, temperatūros pakankamos, kad pasireikštų lėtinio hidridinio pleišėjimo senėjimo mechanizmas. Todėl naudojant šią metodiką galima patobulinti kuro apvalkalų konstrukciją bei panaudoto branduolinio kuro saugojimo procedūras.

Įvertinus radiacijos įtaką cirkonio lydinio savybėms sukurta metodika tinkama ir iradijuotų medžiagų branduolinės energetikos objektų konstrukcinių elementų irimo tąsumui, esant hidridams ir terminiam poveikiui, vertinti.

Atlikus hidridų ir terminio poveikio branduolinės energetikos objektų konstrukcinių elementų irimui skaitinius tyrimus ir atlikus hidridų matmenų matavimus cirkonio lydinyje, galima daryti tokias išvadas:

1. Hidridai kuro kanalo vamzdyje, pagamintame iš TMO-2 Zr-2,5Nb lydinio, linkę susidaryti vamzdžio žiedine-ašine kryptimi. Hidridų matavimai parodė, kad didėjant vandenilio koncentracijai hidridų vidutinis storis, ilgis ir tūrinė dalis cirkonio matricoje didėja, o jų pokytį nuo vandenilio koncentracijos galima aprašyti tiesine funkcija.

2. Sukurtas skaitinis metodas leidžia nustatyti cirkonio lydinio su hidridais tamprumo modulį su 9 % paklaida, o takumo ribą su 14 % paklaida, lyginant su eksperimentinių tyrimų duomenimis.

3. Dvimatis baigtinių elementų modelis naudojant standartinius kompaktinius bandinius netinka medžiagos kritinei irimo tąsumo vertei nustatyti, kadangi nustatyta P_Q vertė plokščios deformacijos būvio atveju nuo eksperimento rezultatų skiriasi 15 %, o plokščio įtempių būvio atveju net 47 %, o naudojant trimatį baigtinių elementų modelį P_Q vertė nuo eksperimento rezultatų skiriasi tik 5 %. Naudojant trimatį baigtinių elementų kompaktinio bandinio modelį nustatytos cirkonio lydinio su hidridais

61

kritinės įtempių intensyvumo koeficiento vertės lyginant su eksperimento duomenimis nesiskiria daugiau kaip 10 %.

4. Naudojant nustatytą antro laipsnio daugianarę funkciją galima įvertinti plyšio padidėjimą kompaktiniame bandinyje. Skaitiškai nustatytas plyšio padidėjimas yra iki 10 % didesnis nei gautas eksperimentiškai.

5. Cirkonio lydinio su hidridais skaitiškai nustatytos kritinės J-integralo vertės J_{IC}, lyginant su eksperimento duomenimis, didesnės iki 20 %, kai vandenilio koncentracija lydinyje yra mažesnė nei 52 ppm. Didėjant vandenilio koncentracijai didėja ir skaitinio nustatymo paklaida. Todėl skaitinio vertinimo metodiką ir nustatytą daugianarę funkciją rekomenduojama naudoti TMO-2 Zr-2,5Nb lydinio irimo tąsumui vertinti iki 52 ppm vandenilio koncentracijos ribos.